Unified approach to electrical and thermal transport in high-T_c superconductors

Rufus Boyack,[1] Zhiqiang Wang[,2] Qijin Chen[,3] and K. Levin[2]

[1]*Département de Physique, Université de Montréal, Montréal, Québec H3C 3J7, Canada*
[2]*James Franck Institute, University of Chicago, Chicago, Illinois 60637, USA*
[3]*Hefei National Laboratory for Physical Sciences at the Microscale*
University of Science and Technology of China, Shanghai 201315, China

In this paper, we present a consolidated equation for all low-field transport coefficients, based on a reservoir approach developed for noninteracting quasiparticles. This formalism allows us to treat the two distinct types of charged (fermionic and bosonic) quasiparticles that can be simultaneously present, as, for example, in superconductors. Indeed, in the underdoped cuprate superconductors, these two types of carriers result in two onset temperatures with distinct features in transport: T^*, where the fermions first experience an excitation (pseudo)gap, and T_c, where bosonic conduction processes are dominant and often divergent. This provides the central goal of this paper, which is to address the challenges in thermoelectric transport that stem from having two characteristic temperatures as well as two types of charge carriers whose contributions can in some instances enhance each other and in others compete. We show how essential features of the cuprates (their bad-metal character and the presence of Fermi arcs) provide an explanation for the classic pseudogap onset signatures at T^* in the longitudinal resistivity, ρ_{xx}. Based on the fits to the temperature-dependent ρ_{xx}, we present the implications for all of the other thermoelectric transport properties.

I. INTRODUCTION

There is renewed interest in thermoelectric transport properties in the condensed matter community, motivated in part by the refined experimental capabilities which address the difficult measurements [1–5] of the small thermal Hall effect. The thermal Hall effect has attracted additional excitement because of topological signatures [2,6,7] which we now understand can be embedded in these data. Moreover, with better experimental understanding of strongly correlated materials, such as the high-temperature superconductors, this has called attention to the need to understand transport properties in a holistic way, rather than to focus on any particular quantity alone. Among the issues of interest [8–10] are subtle but important features related to magnetization effects, which must be incorporated in a proper treatment of thermoelectric transport properties.

This leads to the goal of the present paper, which is to address the full complement of transport coefficients in the normal-state ($T > T_c$) of strongly correlated superconductors, focusing on the weak magnetic field regime. We assume that this normal state is characterized by a mixture of fermions and fluctuating Cooper pairs. However, in contrast to conventional fluctuation theory [11], the fermions themselves are under the influence of pairing fluctuations and this in turn feeds back to renormalize the pairs. Both components contribute to the thermoelectric transport properties, and when the two are treated as noninteracting quasiparticles, we demonstrate, quite remarkably, that their contributions can be consolidated into a single equation for all transport coefficients.

Our derivation of the transport coefficients is based on the introduction of a grand-canonical reservoir containing localized, charged particles (such as proposed by Caldeira and Leggett [12]) which can be either bosonic or fermionic. We couple the reservoir to a system (consisting of either noninteracting fermions or bosons) with the same statistics. Because the principal system is open, dissipation is automatically generated in the transport expressions after integrating out the reservoir degrees of freedom. Furthermore, this approach allows a more direct treatment of temperature gradient perturbations and enables us to avoid the complications of Luttinger's [13] gravitational potential approach for deriving thermal transport coefficients. Our single equation for the full set of thermoelectric transport coefficients depends only on the particle spectral functions. Importantly, our formulas have properly taken into account the magnetization currents [8–10] and satisfy the Onsager reciprocal relations.

In the mixture of fermions and fluctuating Cooper pairs, these latter, bosonic contributions are often described by Gaussian fluctuation theory. This paper goes beyond this conventional fluctuation scheme. The framework we use [14] can be interpreted as an extension of self-consistent Hartree fluctuation theory [15,16], which produces a pairing-induced pseudogap in the fermionic energy spectrum. We define the onset temperature of this pseudogap as T^*, which can be larger than T_c by orders of magnitude as the pairing attraction becomes progressively stronger. The formation of the pseudogap reflects the fact that electrons and fluctuating Cooper pairs are strongly intertwined. Both contributions to transport should be considered simultaneously.

While in this paper we emphasize both fermionic and bosonic transport contributions, the literature in the cuprates exhibits a kind of dichotomy. There has been a focus on theories in which the transport is dominated by bosonic contributions where T^* plays no role. These derive from conventional Gaussian fluctuations [17–22], which are important in the immediate vicinity of T_c. Additionally, there has been a focus on transport associated with pseudogapped fermions [23–25], where T_c plays little or no role. For this case, however, a variety of different origins of the pseudogap have been contemplated.

Here we argue that both the fluctuating Cooper pairs and pseudogapped fermions should be present in strongly correlated superconductors. Moreover, if the pseudogap is due to pairing fluctuations, the pairs and fermions are not independent. Thus, we find the size of the fermionic gap reflects the bosonic binding energy and constrains the number of preformed pairs. Due to the finite lifetime of these pairs, and their d-wave pairing nature, the pseudogap leads to a broadening of the nodes in the fermionic energy spectrum, which can, in the cuprates, be associated with Fermi arcs [26].

Given that both the fermions and bosons contribute to thermoelectric transport, a key question with strong experimental implications is: Under what circumstances can the bosonic transport contributions be visible, as compared to those from the fermions, at relatively high temperatures around T^*? Interestingly, we find that the bad-metal character of the cuprates enables the bosonic terms to dominate their fermionic counterparts, making the former more evident well outside the conventional fluctuation regime. We illustrate these points using a Fermi arc + preformed Cooper pair model for the cuprates. To constrain the phenomenological parameters in our model, we fit the theoretical temperature-dependent DC resistivity, $\rho_{xx}(T)$, to that of a typical cuprate with a pseudogap. This serves to disentangle the relative weights of the fermionic and bosonic contributions; we then outline the resulting implications for the entire complement of transport properties.

As one last argument for our more holistic approach to transport, we note that this enables us to quantitatively evaluate the open-circuit corrections to transport coefficients. These have recently been of interest [27] in the context of thermal Hall measurements. Here, we quite generally quantify these contributions and find that they are negligibly small.

The remainder of the paper is organized as follows. In Sec. II, we define transport coefficients in general and discuss their symmetry properties. In Sec. III, we present our theoretical formalism and results for the bosonic thermoelectric transport. Section IV reviews our strong-pairing fluctuation theory. The inclusion of the fermionic contributions is discussed in Sec. V, while an overview of the numerical results appears in Sec. VI. Section VII contains estimates of the usually neglected open-circuit correction terms using our numerical approach as well as experimental data on the cuprates. We conclude our paper with Sec. VIII. In addition, we make a number of details available in several appendices. Appendix A gives a summary of transport in conventional superconducting fluctuation theory; Appendix B presents a comparison of transport in bad and good metals. Finally, Appendices C and D provide detailed comparisons between our numerical results

(for the physical case of highly resistive or bad metals) and cuprate experiments.

II. GENERAL ASPECTS OF TRANSPORT THEORY

A. General transport coefficients

The transport coefficients are defined within linear-response theory, where the external perturbations consist of an electric field $\mathbf{E}$ and a temperature gradient $\mathbf{\Theta} = -\nabla T$. The pertinent equations for the (transport) electric current $\mathbf{J}^e_{\mathrm{tr}}$ and the (transport) heat current $\mathbf{J}^h_{\mathrm{tr}}$ are defined in terms of these coefficients by

$$\mathbf{J}^e_{\mathrm{tr}} = \overleftrightarrow{\sigma}\mathbf{E} + \overleftrightarrow{\beta}\mathbf{\Theta}, \quad \mathbf{J}^h_{\mathrm{tr}} = \overleftrightarrow{\gamma}\mathbf{E} + \overleftrightarrow{\kappa}\mathbf{\Theta}. \quad (2.1)$$

The electrical conductivity tensor is denoted by $\overleftrightarrow{\sigma}$, the thermal conductivity tensor is $\overleftrightarrow{\kappa}$, and the thermoelectric tensors are $\overleftrightarrow{\beta}$ and $\overleftrightarrow{\gamma}$. Solving Eqs. (2.1) for $\mathbf{E}$ gives

$$\mathbf{E} = \overleftrightarrow{\sigma}^{-1}(\mathbf{J}^e_{\mathrm{tr}} - \overleftrightarrow{\beta}\mathbf{\Theta}). \quad (2.2)$$

As discussed in Refs. [13,28–30], thermal and thermoelectric response measurements are carried out under open-circuit conditions, where the transport electric current is set to zero: $\mathbf{J}^e_{\mathrm{tr}} = 0$. In the absence of a particle current, Eq. (2.2) shows that a nonzero temperature gradient produces an electric field. This can be understood physically from the fact that a temperature gradient causes a diffusion of particles, which then sets up the field.

The thermopower tensor, denoted by $\overleftrightarrow{S}$, is an important transport quantity, and it is defined [11,31] by expressing Eq. (2.2) as $\mathbf{E} = \overleftrightarrow{\rho}\mathbf{J}^e_{\mathrm{tr}} - \overleftrightarrow{S}\mathbf{\Theta}$, where $\overleftrightarrow{\rho}$ is the resistivity tensor. Comparing this expression with Eq. (2.2) gives

$$\overleftrightarrow{\rho} = \overleftrightarrow{\sigma}^{-1}, \quad (2.3)$$

$$\overleftrightarrow{S} = \overleftrightarrow{\sigma}^{-1}\overleftrightarrow{\beta} = \overleftrightarrow{\rho}\overleftrightarrow{\beta}. \quad (2.4)$$

In the presence of an external magnetic field $\mathbf{B} = B\hat{z}$ [perpendicular to the two-dimensional (2D) system], the transverse components of these tensors are nonzero and of considerable interest. The transverse resistivity, ρ_{yx}, measured in the absence of a temperature gradient, is related to the Hall coefficient R_{H} via $\rho_{yx} = BR_{\mathrm{H}}$. This is given in terms of the components of the electrical conductivity by

$$R_{\mathrm{H}} = \frac{\rho_{yx}}{B} = \frac{1}{B}\frac{\sigma_{xy}}{\sigma_{xx}^2 + \sigma_{xy}^2}. \quad (2.5)$$

Similarly, the transverse thermopower is related to the Nernst coefficient, ν, via $S_{yx} = -B\nu$, with

$$\nu = -\frac{S_{yx}}{B} = \frac{1}{B}\left(\frac{\beta_{xy}\sigma_{xx} - \beta_{xx}\sigma_{xy}}{\sigma_{xx}^2 + \sigma_{xy}^2}\right). \quad (2.6)$$

Another important transverse transport quantity is the thermal Hall conductivity. Setting $\mathbf{J}^e_{\mathrm{tr}}$ to zero in Eq. (2.2) and then inserting this expression for the electric field into Eqs. (2.1) yields a heat current:

$$\mathbf{J}^h_{\mathrm{tr}} = [\overleftrightarrow{\kappa} - \overleftrightarrow{\gamma}\overleftrightarrow{\sigma}^{-1}\overleftrightarrow{\beta}]\mathbf{\Theta} \equiv \overleftrightarrow{\overleftrightarrow{\kappa}}\mathbf{\Theta}. \quad (2.7)$$

The last equivalence defines the measured thermal conductivity tensor $\overleftrightarrow{\overleftrightarrow{\kappa}}$ via Fourier's law of heat conduction. Written out

explicitly, the thermal Hall conductivity is

$$\widetilde{\kappa}_{xy} = \kappa_{xy} - T \frac{(\beta_{xy}^2 - \beta_{xx}^2)\sigma_{xy} + 2\beta_{xx}\sigma_{xx}\beta_{xy}}{\sigma_{xx}^2 + \sigma_{xy}^2}, \qquad (2.8)$$

where use has been made of the Onsager relations between $\overleftrightarrow{\gamma}$ and $\overleftrightarrow{\beta}$. This expression highlights how understanding thermal transport requires knowledge of the magnitude of both the electrical and thermoelectric conductivities. These interconnections between electrical and thermal response serve to emphasize the value of a unified theory that deals with all transport coefficients simultaneously.

B. Onsager relations and particle-hole symmetry

Due to time-reversal symmetry in the underlying equations of motion, the transport coefficient tensors in Eqs. (2.1) obey the following Onsager reciprocal relations: $\sigma_{ij}(\mathbf{B}) = \sigma_{ji}(-\mathbf{B})$, $\beta_{ij}(\mathbf{B}) = \gamma_{ji}(-\mathbf{B})/T$, and $\kappa_{ij}(\mathbf{B}) = \kappa_{ji}(-\mathbf{B})$.

These coefficients additionally possess particle-hole transformation properties. The particle-hole symmetry operator is denoted by $\mathcal{C}$. Under the action of this operator, $\mathbf{E} \to -\mathbf{E}$, $\mathbf{B} \to -\mathbf{B}$, and $\mathbf{J}_{\text{tr}}^e \to -\mathbf{J}_{\text{tr}}^e$, whereas T and $\mathbf{J}_{\text{tr}}^h$ are invariant. Using these relations in Eqs. (2.1), the transformation properties for the transport coefficients are $\mathcal{C}\sigma(\mathbf{B})\mathcal{C}^{-1} = \sigma(-\mathbf{B})$, $\mathcal{C}\beta(\mathbf{B})\mathcal{C}^{-1} = -\beta(-\mathbf{B})$, and $\mathcal{C}\kappa(\mathbf{B})\mathcal{C}^{-1} = \kappa(-\mathbf{B})$. From these relations it follows that a particle-hole symmetric system has $\beta_{xx} = \sigma_{xy} = \kappa_{xy} = 0$.

III. TRANSPORT COEFFICIENTS FOR NONINTERACTING PARTICLES

In this section, we present a methodology that enables all of the transport coefficients in Eqs. (2.1) to be expressed in terms of a simple formula that depends only on the relevant spectral functions and associated vertex functions. This theory applies to free bosonic and fermionic theories, with arbitrary single-band dispersion relations that preserve time-reversal, spatial inversion, and rotation symmetries. It is thus applicable to the bosonic contribution in the Ginzburg-Landau (GL) fluctuation theory of superconductors [11], as well as to a strong-pairing fluctuation theory [14] that incorporates a normal-state cuprate pseudogap, to be discussed in Sec. IV.

For concreteness, we first consider the case of noninteracting bosons, presenting an outline of the derivation and leaving a more detailed exposition to a forthcoming paper. This paper is based on an approach first introduced in Ref. [32].

To derive the coefficients in Eqs. (2.1), we couple our principal system to a Caldeira-Leggett thermal reservoir with localized particles [32]. The reservoir particles have the same types of charge and statistics as those of the principal system. The system achieves equilibrium by exchanging particles and energy with the reservoir. Applying a perturbation, either $\mathbf{E}$ or $\boldsymbol{\Theta}$ in the presence of the magnetic field $\mathbf{B}$, one can write down the equation of motion for both the principal system and the reservoir particles in the presence of the perturbation, and then integrate out the reservoir particles by absorbing their effects as a phenomenological local self-energy into the definition of the Green's function associated with the principal system. Using these perturbed Green's functions, we then compute the microscopic current densities, $\langle \hat{\mathbf{J}}^e \rangle_{\mathbf{E},\boldsymbol{\Theta}}$ and $\langle \hat{\mathbf{J}}^h \rangle_{\mathbf{E},\boldsymbol{\Theta}}$, to linear

order in $\mathbf{E}$ or $\boldsymbol{\Theta}$ and in $\mathbf{B}$, which can be written compactly as

$$\begin{bmatrix} \langle \hat{\mathbf{J}}^e \rangle_{\mathbf{E},\boldsymbol{\Theta}} \\ \langle \hat{\mathbf{J}}^h \rangle_{\mathbf{E},\boldsymbol{\Theta}} \end{bmatrix} = \begin{bmatrix} \overleftrightarrow{L}_{e,e} & \overleftrightarrow{L}_{e,h} \\ \overleftrightarrow{L}_{h,e} & \overleftrightarrow{L}_{h,h} \end{bmatrix} \begin{bmatrix} \mathbf{E} \\ \boldsymbol{\Theta} \end{bmatrix}. \qquad (3.1)$$

Here, $\hat{\mathbf{J}}^e$ and $\hat{\mathbf{J}}^h$ are the electric and heat current density operators; $\overleftrightarrow{L}_{e,e}$, $\overleftrightarrow{L}_{e,h}$, $\overleftrightarrow{L}_{h,e}$, and $\overleftrightarrow{L}_{h,h}$ are four tensorial coefficients, which can be fully expressed in terms of the particle's Green's functions, retarded and/or advanced.

It is well known that the microscopic currents in Eq. (3.1) are a subset of the macroscopic transport currents in Eqs. (2.1) [9,10]. To obtain the transport currents, one needs to subtract the divergence-free currents due to the charge magnetization $\mathbf{M}^e$ and the heat magnetization $\mathbf{M}^h$. As elaborated in Refs. [9,10], in the presence of $\mathbf{E}$ or $\boldsymbol{\Theta}$ perturbations, the correct subtractions are

$$\begin{bmatrix} \mathbf{J}_{\text{tr}}^e \\ \mathbf{J}_{\text{tr}}^h \end{bmatrix} = \begin{bmatrix} \overleftrightarrow{L}_{e,e} & \overleftrightarrow{L}_{e,h} - \frac{\partial \mathbf{M}^e}{\partial T} \times \\ \overleftrightarrow{L}_{h,e} - \mathbf{M}^e \times & \overleftrightarrow{L}_{h,h} - \frac{\partial \mathbf{M}^h}{\partial T} \times \end{bmatrix} \begin{bmatrix} \mathbf{E} \\ \boldsymbol{\Theta} \end{bmatrix}. \qquad (3.2)$$

The transport coefficients are then defined by comparing this equation with Eq. (2.1). The magnetization currents for the thermoelectric tensors $\overleftrightarrow{\beta}$ and $\overleftrightarrow{\gamma}$, the off-diagonal magnetization terms in Eq. (3.2), were first derived by Obraztsov [8]. Including these magnetization currents is vital to ensure the Onsager reciprocal relations and the laws of thermodynamics are obeyed [9,10].

In our reservoir approach, we express both $\overleftrightarrow{L}_{ij}$ and $\mathbf{M}^i$, with $\{i, j\} \in \{e, h\}$, in terms of Green's functions. Although each of the two generally involves complicated combinations of retarded and advanced Green's functions, the final answers for the transport coefficients on the right-hand side of Eq. (3.2) turn out to be simply written in terms of spectral functions and current vertices. We find that the matrix appearing in Eq. (3.2) can be consolidated [32] into the form

$$J_{(\text{tr})a}^n = \sum_{n'=0}^{1} \sum_b \mathcal{L}_{ab}^{nn'} E_b^{n'}, \qquad (3.3)$$

with

$$\mathcal{L}_{ab}^{nn'} = \int \frac{d^2p}{(2\pi)^2} \frac{dz}{2\pi} z^{n+n'} \left[\frac{q^{2-n-n'}}{2T^{n'}} v_a v_b A_b^2(z, \mathbf{p}) \right.$$
$$\left. + \frac{q^{3-n-n'}}{6T^{n'}} B \epsilon_{cd} v_a v_c v_{bd} A_b^3(z, \mathbf{p}) \right] b^{(1)}(z). \qquad (3.4)$$

Here, $A_b(z, \mathbf{p})$ is the bosonic spectral function. To arrive at this compact form, we have introduced the notation $E_a^0 \equiv E_a$ and $E_a^1 \equiv -\partial_a T$, where $a = \{x, y\}$. Here $b^{(1)}(z) \equiv -\partial b(z)/\partial z$ where $b(z) = (e^{z/T} - 1)^{-1}$ is the Bose-Einstein distribution function (we set $\hbar = k_B = 1$ and will restore these units only when necessary). The relations between $\mathcal{L}_{ab}^{nn'}$ and the coefficients in Eqs. (2.1) are $\sigma_{ab} = \mathcal{L}_{ab}^{00}$, $\beta_{ab} = \mathcal{L}_{ab}^{01}$, $\gamma_{ab} = \mathcal{L}_{ab}^{10}$, and $\kappa_{ab} = \mathcal{L}_{ab}^{11}$.

In Eq. (3.4), z is the real frequency and q is the charge of the particles in the system: $q = -e < 0$ for electrons and $q = -2e$ for fluctuating Cooper pairs. We define v_a as the a-component velocity whose wave vector $\mathbf{p}$ dependence has been suppressed for brevity while v_{ab} is the ab component of the inverse effective-mass tensor, which is also $\mathbf{p}$ dependent. In the second term of Eq. (3.4), ϵ_{cd} is the 2D Levi-Civita symbol. Because of the underlying spatial inversion and rotation

symmetries of the band dispersion, the first term in Eq. (3.4) is longitudinal, while the second term is transverse.

A few comments are in order concerning Eq. (3.4), as it might seem rather unexpected that there exists a single, closed-form, Kubo-like expression from which all of the transverse and longitudinal transport coefficients can be obtained. Notably, for the transverse contribution, this result also includes magnetization corrections in addition to the intrinsic $\overleftrightarrow{L}_{ij}$ terms. That this is possible partially follows from confining our attention to the weak magnetic field limit.

We note that from Eq. (3.4) it is easy to verify consistency with the Onsager reciprocal relations, i.e., $T^{n'}\mathcal{L}_{ab}^{nn'}(\mathbf{B}) = T^n\mathcal{L}_{ba}^{n'n}(-\mathbf{B})$ (no summation). We emphasize that this result is a consequence of including the magnetization terms in Eq. (3.2).

Next we briefly compare our approach to other methods in the literature. In a classic series of papers, Luttinger [13,29] developed an approach which requires introducing a source ψ for perturbations in the energy density, in analogy with the way the vector potential **A** is used to initiate changes in the electric current. The field ψ acts as a source that enables describing a local temperature $T(\mathbf{r})$, which is distinct from the equilibrium temperature. This formalism builds on the Einstein relation which asserts that coefficients of gradients in ψ and T must be equal; this is analogous to the other well-known Einstein relation that coefficients of gradients in chemical potential μ and electric potential ϕ are the same for electrical response [9,31]. The Luttinger approach was implemented in more detail by Cooper *et al.* [9], who derived the magnetization current contributions for all of the transport coefficients.

While our formalism is different, we equivalently include these same magnetization current effects here. We emphasize that in our approach to electrical and thermal transport the thermal response is naturally deduced from temperature fluctuations about the equilibrium temperature set by the reservoir. The advantages of the heat-reservoir approach are that it provides a direct method to derive thermal transport, avoiding the more abstract and technically difficult Luttinger formalism. In this way, we formulate the theory with $\nabla\psi = 0$ from the outset.

IV. TRANSPORT DUE TO STRONG-PAIRING FLUCTUATIONS: BOSONS WITH PSEUDOGAP EFFECTS

We apply the general expression for transport coefficients in Eq. (3.4) to a model that consists of a mixture of fluctuating Cooper pairs and electrons to address transport properties of the pseudogapped normal state of cuprates [33]. In reality the fluctuating pairs and electrons are constantly interconverting. Importantly, the effects of this interconversion can be treated in a self-consistent, mean-field manner, where they are manifested as a pseudogap in the electron energy spectrum. This excitation gap, at the same time, feeds back to alter the general physical properties of the Cooper pairs.

A. Preformed pairs and the pseudogap

The observations that the pseudogap is associated with a reduction in carrier number [34] have led many to argue

against the concept of preformed pairs as the origin of the pseudogap. Indeed, the notion that the pseudogap arises in this way has gone in and out of favor with time. Indications for some unspecified form of additional order which onsets at T^*, as well as alternative experiments, have more recently been cited as evidence against a preformed-pair theory. Among these experiments are (i) evidence for two-gap physics [35] in which the nodal and anti-nodal gaps have different temperature dependences, and (ii) the existence of Fermi arcs was also argued to be difficult to understand [36], at least within one preformed-pair framework. Finally, (iii) there are claims of particle-hole asymmetry in the fermionic quasiparticle energy dispersion in the pseudogap phase [37], although this is not substantiated by other experiments [38,39].

In this paper, we explore the field-dependent transport in a preformed-pair scenario. Here we are motivated by the anomalously high transition temperatures which support the view that the cuprates are in an intermediate state between BCS and Bose-Einstein condensation (BEC) [40]. Importantly, there is well-supported evidence that in the strong-pairing preformed-pair theory the observations (i) and (ii) are in fact fully consistent. For point (i), a number of references address the two gap dichotomy [41,42], while the presence of Fermi arcs is addressed in this paper. We emphasize that there are multiple flavors of preformed-pair scenarios; the one we consider here has a laboratory realization in ultracold Fermi gas superfluids [14]. An alternative scenario is the phase-fluctuation picture of Emery and Kivelson [43]. At the very least, the strong-pairing approach that we adopt represents a rather benign extension of BCS theory, which appears warranted due to the short coherence length.

We emphasize that the physical picture introduced in this paper can also be seen as a natural generalization of self-consistent-Hartree approaches [15,16] to the time-dependent GL framework [44]. These have been independently advocated [19] for addressing cuprate transport.

B. Theoretical approach to strong-pairing fluctuations

Our approach to preformed-pair theory is, in some sense, a generalization of conventional superconducting fluctuation theory (see Appendix A). The latter, however, does not explicitly incorporate pseudogap effects, which we argue are associated with stronger-than-BCS attractive interactions. One expects, as the pairing strength increases, the inverse fluctuation propagator transitions from a predominantly diffusive to a propagating form, which we write as

$$t_R^{-1}(z, \mathbf{p}) = Z[\kappa z - \mathbf{p}^2/(2M_{\text{pair}}) - |\mu_{\text{pair}}| + i\Gamma z], \quad (4.1)$$

where $\{Z, \kappa, \Gamma\}$ are all real. This expression breaks particle-hole symmetry due to the presence of the κz term. We will find that κ, which is equal to ± 1 here, plays an important role in the transport coefficients β_{xx}, σ_{xy}, and κ_{xy}. In conventional fluctuation theories the counterpart to κ is small.

We now give a brief overview of the formalism that we use to arrive at the pair propagator (or t matrix), t_R in Eq. (4.1). This is based on a BCS-like structure, extended to include stronger attractive interactions. We are motivated by the observation that, in BCS theory, the gap equation (here considered

for d-wave pairing symmetry),

$$0 = \frac{1}{g} + \sum_{\mathbf{k}} \frac{1 - 2f(E_{\mathbf{k}})}{2E_{\mathbf{k}}} \varphi_{\mathbf{k}}^2, \tag{4.2}$$

can be understood as a Thouless criterion reflecting a $q = 0$ divergence of a dressed t matrix [14], with inverse

$$t^{-1}(p) = \sum_{k} G(k) G_0(p - k) \varphi_{\mathbf{k} - \mathbf{p}/2}^2 + g^{-1}. \tag{4.3}$$

Here $f(x)$ is the Fermi-Dirac distribution function.

In Eq. (4.2), $g < 0$ is the strength of the attractive d-wave pairing interaction $V_{\mathbf{k},\mathbf{k}'} = g\varphi_{\mathbf{k}}\varphi_{\mathbf{k}'}$, where $\varphi_{\mathbf{k}} = \cos k_x - \cos k_y$ is the d-wave pairing form factor; $E_{\mathbf{k}} = \sqrt{\xi_{\mathbf{k}}^2 + \Delta_{\text{mf}}^2 \varphi_{\mathbf{k}}^2}$ and the underlying bare fermion dispersion is $\xi_{\mathbf{k}} = \epsilon_{\mathbf{k}} - \mu_F$, where μ_F is the fermionic chemical potential. Here, Δ_{mf} is the temperature-dependent BCS mean-field (mf) gap. In Eq. (4.3), $G_0(k) = (i\omega_n - \xi_{\mathbf{k}})^{-1}$ and $G(k) \equiv [G_0^{-1}(k) - \Sigma(k)]^{-1}$ are the bare and dressed fermionic Green's functions, respectively, where $\Sigma(k) = -(\Delta_{\text{mf}}\varphi_{\mathbf{k}})^2 G_0(-k)$ is the superconducting self-energy. We define $k = (i\omega_n, \mathbf{k})$ and $p = (i\Omega_m, \mathbf{p})$ as two four-vectors with $\omega_n = (2n + 1)\pi T$ and $\Omega_m = 2m\pi T$.

The t matrix in Eq. (4.3) involves one bare and one dressed Green's function, as has been recognized in the literature [45,46]. If one expands $t^{-1}(p)$ at $p = 0$ in a Taylor expansion and analytically continues the result to real frequencies, as in Eq. (4.1), one finds that the Thouless criterion, $t^{-1}(p = 0) = 0$, can be regarded as a BEC condition for the pair chemical potential: $\mu_{\text{pair}} = 0$ for all $T \leqslant T_c$.

We note that this BEC condition describes the approach to condensation from above T_c. In this way, one should view the associated t matrix in the Thouless criterion as characterizing the noncondensed pairs. To extend this approach to strong pairing, we use the same t matrix as in Eq. (4.3) but with a crucial difference from strict BCS theory in the fermion self energy $\Sigma(k)$. In general t-matrix theories, and ours in particular,

$$\Sigma(k) = \sum_{p} t(p) G_0(p - k) \varphi_{\mathbf{k} - \mathbf{p}/2}^2. \tag{4.4}$$

Here we represent the noncondensed pairs through contributions from the $q \neq 0$ component of $t(q)$. By numerically solving the coupled Eqs. (4.3) and (4.4), one can determine $t(q)$. This is, however, very challenging.

For this reason, we adopt the so-called pseudogap (pg) approximation, in which one observes that $t(p)$ is strongly peaked about $p = 0$ so one can approximate $t(p)$ in Eq. (4.3) (after analytical continuation) by the form of $t_R(z, \mathbf{p})$ in Eq. (4.1). Simultaneously, the approximate self-energy due to the noncondensed pairs is given by $\Sigma(k) \approx -(\Delta_{\text{pg}}\varphi_{\mathbf{k}})^2 G_0(-k)$, with

$$\Delta_{\text{pg}}^2(T) = -\sum_{p \neq 0} t(p), \quad T \lesssim T_c. \tag{4.5}$$

Note the $p = 0$ component of $t(p)$ (which corresponds to the condensate) is necessarily excluded in the above summation. The above approximation is valid for $|\mu_{\text{pair}}|$ very small, that is, below or only slightly above T_c. Precisely at $T = T_c$, all pairs are noncondensed and thus the condition $\mu_{\text{pair}} = 0$ requires [14] that $\Delta_{\text{pg}}(T_c) = \Delta_{\text{mf}}(T_c)$.

The focus of this paper is, however, on transport in the normal state over the entire temperature range between T_c and T^*. Indeed, one observes that $T^* \gg T_c$ when the pairing is strong. In contrast to the above treatment for $T \lesssim T_c$, which has a rather precise microscopic basis [14], we must make some simple but physical assumptions to extend it well away from T_c. We assume that in the normal state,

$$\Delta_{\text{pg}}(T) = \Delta_{\text{mf}}(T), \quad T \geqslant T_c. \tag{4.6}$$

As a consequence, Δ_{pg} vanishes at the mean-field transition temperature, which we associate with T^*, although, strictly speaking, there should be a gentle crossover to zero here.

We solve Eq. (4.2) together with the electron density constraint equation,

$$n_e = \sum_{\mathbf{k}} \left[1 - \frac{\xi_{\mathbf{k}}}{E_{\mathbf{k}}} \tanh\left(\frac{E_{\mathbf{k}}}{2T}\right) \right], \tag{4.7}$$

to determine $\Delta_{\text{mf}}(T)$ and the fermionic chemical potential $\mu_F(T)$ for given $\{g, T, n_e\}$. The coupling constant g is chosen to give the desired T^*. With Δ_{mf} for the excitation gap determined, we can then derive [47] M_{pair} and Z from the strong-pairing t matrix in Eq. (4.3).

This group of assumptions is rather benign, as it guarantees continuity between the normal-state results and those at T_c. However, understanding μ_{pair} in the normal state is more subtle. There is no reliable way of computing μ_{pair} for the whole temperature range $T_c < T < T^*$ in a self-consistent manner. Here, we take a more phenomenological approach by interpolating results of μ_{pair} in the two limits $T \to T_c$ and $T \to T^*$. For T slightly above T_c, we presume that μ_{pair} is well described by the conventional fluctuation behavior, namely, $\mu_{\text{pair}} \approx (8/\pi)(T_c - T)$ [11]. This will be justified later in the paper through a comparison of the calculated longitudinal resistivity with corresponding experiments. In the other limit, $T \to T^*$, the number of pairs vanishes, which requires that $\mu_{\text{pair}} \to -\infty$. A formula for μ_{pair} that satisfies these requirements and that smoothly interpolates between the two limits is [48]:

$$\mu_{\text{pair}} = \frac{8}{\pi}(T^* - T_c) \ln \frac{T^* - T}{T^* - T_c}. \tag{4.8}$$

We emphasize that our results are not in detail sensitive to this particular interpolation.

C. Transport coefficients in the small $|\mu_{\text{pair}}|$ limit

The central quantity for calculating the bosonic contribution to transport coefficients is the bosonic spectral function A_b which appears in Eq. (3.4). This is defined in terms of the retarded pairing fluctuation propagator t_R as [49]

$$A_b(z, \mathbf{p}) = \text{Re}[2it_R(z, \mathbf{p})]. \tag{4.9}$$

The velocity components in Eq. (3.4) are defined by $v_a(\mathbf{p}) \equiv -\partial t_R^{-1}(z, \mathbf{p})/\partial p_a = Zp_a/M_{\text{pair}}$, which constitutes a Ward identity [50,51]; similarly, the inverse effective-mass component $v_{ab}(\mathbf{p}) \equiv -\partial^2 t_R^{-1}(z, \mathbf{p})/(\partial p_a \partial p_b) = Z/M_{\text{pair}}\delta_{ab}$, where δ_{ab} is the Kronecker delta function. With the bosonic parameters $\{M_{\text{pair}}, \mu_{\text{pair}}, Z\}$ determined from the previous section, one can readily evaluate all of the bosonic transport coefficients

from Eq. (3.4). Interestingly, the prefactor Z drops out of the transport coefficients due to a cancellation effect.

For a generic temperature, one needs to resort to numerics to evaluate Eq. (3.4). However, in the limit of $T \to T_c$ and $|\mu_{\text{pair}}|/T_c \ll 1$, when the bosons become critical, an asymptotic formula for the singular contribution of each bosonic transport coefficient can be analytically deduced. Here we insert Eqs. (4.1) and (4.9) into Eq. (3.4) and then expand the Bose-Einstein distribution function derivative for small frequencies. This enables the frequency integral, and subsequently the momentum integral, to be performed analytically.

The final results (for 2D) are

$$\sigma_{xx} = \frac{1}{8\pi} \frac{(\kappa^2 + \Gamma^2)}{\Gamma} \frac{q^2}{\hbar} \frac{k_B T_c}{|\mu_{\text{pair}}|}, \tag{4.10a}$$

$$\beta_{xx} = \frac{1}{4\pi} \frac{\kappa}{\Gamma} \frac{qk_B}{\hbar} \ln\left|\frac{E_\Lambda}{\mu_{\text{pair}}}\right|, \tag{4.10b}$$

$$\kappa_{xx} = \text{constant}, \tag{4.10c}$$

$$\sigma_{xy} = \frac{1}{24\pi} \frac{\kappa(\kappa^2 + \Gamma^2)}{\Gamma^2} \frac{q}{e} \frac{q^2}{\hbar} \frac{\xi_0^2}{\ell_B^2} \frac{(k_B T_c)^2}{|\mu_{\text{pair}}|^2}, \tag{4.10d}$$

$$\beta_{xy} = \frac{1}{24\pi} \frac{(3\kappa^2 + \Gamma^2)}{\Gamma^2} \frac{q}{e} \frac{qk_B}{\hbar} \frac{\xi_0^2}{\ell_B^2} \frac{k_B T_c}{|\mu_{\text{pair}}|}, \tag{4.10e}$$

$$\kappa_{xy} = \frac{1}{4\pi} \frac{\kappa}{\Gamma^2} \frac{q}{e} \frac{k_B^2 T_c}{\hbar} \frac{\xi_0^2}{\ell_B^2} \ln\left|\frac{E_\Lambda}{\mu_{\text{pair}}}\right|, \tag{4.10f}$$

where we have restored the constants $\hbar$ and k_B to make the units explicit. In these equations, $\ell_B = \sqrt{\hbar/eB}$ ($eB > 0$) is the magnetic length, E_Λ is an energy cutoff [15,19], and $\xi_0 \equiv \hbar/\sqrt{2M_{\text{pair}}k_B T_c}$.

V. CONTRIBUTIONS FROM THE PSEUDOGAPPED FERMIONS

In addition to the preformed Cooper pairs, the (pseudo)gapped electrons are also carriers of charge and energy in the normal state of a strongly correlated superconductor. That there are generically two types of contributions to transport is evident from conventional fluctuation theory [11], where gauge invariance requires that both the Aslamazov-Larkin (AL) (bosonic) and Maki-Thompson (MT) plus density of states (DOS) (fermionic) diagrams must be present. In contrast to the conventional MT and DOS contributions, here we emphasize that the normal-state fermions must also acquire an excitation gap.

It is of interest to note that there are several phenomenologically motivated papers which presume two types of carriers. Geshkenbein et al. [52] considered nondispersing bosons of charge $-2e$ arising from electrons in the small anti-nodal regime of the Fermi surface where the fermion dispersion is flat; they also included gapless fermions confined to an extended region around the nodes. This scenario is different from the present physical picture where the fermions and pairs are continuously interconverting as in a chemical equilibrium process. More recently, Lee and collaborators [36] have proposed a model for the high-field case, similar to that in Ref. [52] with localized bosons at the antinodes.

To account for the fermionic contribution to transport, we use an additional consolidated transport coefficient equation similar to Eq. (3.4) but for noninteracting fermions:

$$\mathcal{L}_{ab}^{nn'} = 2 \int \frac{d^2k}{(2\pi)^2} \frac{dz}{2\pi} z^{n+n'} \left[\frac{q^{2-n-n'}}{2T^{n'}} v_a v_b A_f^2(z, \mathbf{k}) \right.$$
$$\left. + \frac{q^{3-n-n'}}{6T^{n'}} B\epsilon_{cd} v_a v_c v_{bd} A_f^3(z, \mathbf{k}) \right] f^{(1)}(z). \tag{5.1}$$

This is essentially the same as in Eq. (3.4) except for the prefactor of 2 from spin degeneracy. Here we define $f^{(1)}(z) = -\partial f(z)/\partial z$ as the Fermi-Dirac function derivative and $A_f(z, \mathbf{k})$ as the fermionic spectral function which can be written in terms of the retarded single-particle fermionic Green's function. The latter is given by

$$A_f(z, \mathbf{k}) = \text{Re}[2iG_R(z, \mathbf{k})]. \tag{5.2}$$

Here the Green's function associated with the pseudogapped fermions is rather generally taken in the literature [53] to be of the form

$$G_R^{-1}(z, \mathbf{k}) = z - \xi_{\mathbf{k}} - \frac{\Delta_{\text{pg}}^2(T)\varphi_{\mathbf{k}}^2}{z + \xi_{\mathbf{k}} + i\gamma} + i\Sigma_0(T), \tag{5.3}$$

where $\xi_{\mathbf{k}}$ is the noninteracting electron dispersion.

Important in Eq. (5.3) is that in addition to a broadened BCS-like self-energy associated with the excitation pseudogap Δ_{pg}, we also include a term $\Sigma_0(T)$ which accounts for the finite lifetime of fermions in the absence of superconducting fluctuations. In our calculation, $\Sigma_0(T)$ is a phenomenological function which is assumed to be linear in T. While its physical origin is under debate, this accounts for the underlying and universally observed linear-in-temperature resistivity in optimal and underdoped cuprates at $T > T^*$. We presume this same term is present both above and below T^*.

At a more microscopic level, in our thermal-reservoir approach leading to Eq. (5.1), Σ_0 can be viewed as a self-energy effect arising from integrating out local reservoir degrees of freedom. This is somewhat problematic for arriving at the pseudogap self energy term in Eq. (5.3) which has a microscopic [14] and phenomenological basis [53]. Strictly speaking, the pseudogap self energy cannot be interpreted in this way because it is $\mathbf{k}$ dependent and nonlocal. Nevertheless, here we apply Eq. (5.1) under the assumption that the pseudogapped fermions can be viewed as independent quasi-particles and define $v_a \equiv \partial \xi_{\mathbf{k}}/\partial k_a$ and $v_{ab} \equiv \partial^2 \xi_{\mathbf{k}}/(\partial k_a \partial k_b)$ in Eq. (5.1) using the bare fermion dispersion. This ignores vertex corrections which have been addressed in previous work [54] and found to be reasonably unimportant. We should note that the vertex corrections in the fermionic transport coefficients were also considered in Ref. [55] in the limit of small fermion scattering rate. (Magnetization corrections, which are crucial in the present paper, however, were not treated, since they were not pertinent in the limit considered.)

A nonzero value of γ in Eq. (5.3) leads to a broadening of the d-wave nodes in the electron energy dispersion. This can be associated with Fermi arcs, which are an important feature of angle-resolved photoemission spectroscopy (ARPES) experiments and associated with the pseudogap of underdoped cuprates [14,53]. Its origin at the microscopic level here is related to the finite lifetime of the non-condensed pairs [14],

which is in stark contrast to the infinite lifetime of condensed pairs at $T < T_c$. While the implications of Fermi arcs for transport properties have been considered before [56,57], these have been restricted to the case where there are no bosons.

We note that in describing the pseudogap state, many other fermionic models have been proposed [53]. Notable is the so-called Yang, Rice, Zhang (YRZ) [58] model, which contains a rather similar form for the fermionic Green's function [54] in Eq. (5.3) but with some important differences. The pseudogap parameter in YRZ is not evidently related to pairing fluctuations and instead of $\xi_{\mathbf{k}}$ in the denominator of the pseudogap self-energy term in Eq. (5.3) the YRZ model introduces a different dispersive parameter ($\epsilon_{\mathbf{k}}^{\mathrm{NN}}$) which contains only nearest-neighbor (NN) hopping without a broadening parameter such as γ. Technically, this is associated with Fermi pockets rather than Fermi arcs as in Eq. (5.3), and related transport theory has focused on zero temperature [23–25] in the absence of bosonic degrees of freedom.

It is useful to add here that we are not concerned in this paper with charge-density wave (CDW) effects in the cuprates. The central focus of our cuprate transport analysis is the pseudogap regime. The CDW regime is in rather limited regions of the phase diagram. It typically spans a limited doping range around the commensurate 1/8 doping; additionally it may be induced by very high magnetic fields. As observed in Ref. [59], the pseudogap and charge order are separate phenomena. Thus, our argument for focusing on the pseudogap and pairing effects is that they are an even more robust feature of the cuprates than the CDW-ordered phases.

VI. NUMERICAL RESULTS

A. Overview

We have emphasized that in strongly correlated superconductors it is important to study both bosonic and fermionic contributions to transport. The bosonic terms will tend to have a singular structure near T_c and even possibly contribute to transport at temperatures as high as T^*. Very near T_c, this singular structure is similar to the predictions from GL fluctuation theory.

Our approach to transport builds on rather general assumptions related to claims in the experimental literature. The effect of the pseudogap onset on the fermions is to lead to a decrease in effective fermionic carrier density; this corresponds to a tendency toward an *upturn* in ρ_{xx} which sets in with decreasing temperature, T, below T^*. This upturn is inferred from the behavior of the resistivity $\rho_{xx}(T)$ in cuprates when the superconductivity is suppressed by three different mechanisms—high magnetic fields, B [34,60], extreme underdoping [61], and the destruction of superconductivity due to Zn impurities [62,63].

These experiments are relevant to the behavior of the fermionic channel in the superconducting cuprates due to the widely held belief that such experiments, in particular those at high fields, reveal the pristine character of the pseudogap. Importantly, though, what is observed as the signature of the cuprate pseudogap in $\rho_{xx}(T)$ for the normal phase is a *downturn* which sets in at T^* with decreasing T. This could

be understood if [as in Eq. (4.8)], due to stronger pairing attraction, the bosons are present and contribute to transport away from the critical regime.

In this section, we show the above finding, concerning a form of high-temperature bosonic paraconductivity, is a consequence of the fact that cuprates possess two important features: they are bad metals, and, importantly, also their d-wave pseudogap is associated not with gap nodes but with Fermi arcs. The first of these implies that the fermions play a dominant role in the resistivity or, equivalently, a more minimal role in the conductivity. As a result of the Fermi arcs, the fermionic tendency to enhance the resistivity starting at T^* is suppressed.

Our calculations depend on several phenomenological parameters, including $\{\gamma, \Sigma_0\}$ in Eq. (5.3) and Γ in Eq. (4.1). The broadening parameter γ, in part, sets the length of the Fermi arc in Eq. (5.3) (the Fermi arc length also depends on Σ_0, but the dependence is weak). As is compatible with ARPES measurements, we consider $\gamma = \widetilde{\gamma} T$ [26,53,64,65], with the dimensionless parameter $\widetilde{\gamma} = 3.2$. We determine the remaining two parameters, Σ_0 and Γ, by fitting ρ_{xx} to the corresponding experimental data of a typical cuprate with a pseudogap. Using those constrained parameters, we then calculate all of the other transport coefficients.

For the fermionic calculation, we use $\xi_{\mathbf{k}} = 2t[2 - \cos k_x - \cos k_y] - 4t'[1 - \cos k_x \cos k_y] - \mu_F$ for the dispersion in Eq. (5.3) with $t'/t = 0.35$. Here μ_F is adjusted to give an electron density $n_e = 0.85$ per $\mathrm{CuO_2}$ square, i.e., hole doping $p = 1 - n_e = 15\%$. For definiteness, we choose $t = 75$ meV.

B. Longitudinal resistivity ρ_{xx}

The resistivity of underdoped cuprates typically exhibits a linear-in-T behavior at high temperature $T > T^*$, deriving from a presently unknown mechanism. As temperature is decreased there comes a point (T^*) when the resistivity exhibits a slight downturn from linearity which is maintained until essentially at the transition temperature T_c where it plummets to zero. As is conventional, we take this downturn onset to be a signature of the entrance into the pseudogap phase.

We divide the following discussion into the temperature ranges above and below T^*. Above T^*, to phenomenologically accommodate the linearity of ρ_{xx} in T we use $\Sigma_0(T) = \Gamma_0 + bT$ for the normal state (fermionic) inverse lifetime in Eq. (5.3), where Γ_0 and b are two T-independent constants. Γ_0 characterizes the extrapolated residual resistivity. Γ_0 and b are chosen so that ρ_{xx} at $T > T^*$ fits the experimental data of a nearly optimally doped $\mathrm{Bi_2Sr_2CaCu_2O_{8+\delta}}$ sample in Ref. [66], as shown in Fig. 1. Note that above T^* there is no bosonic contribution to ρ_{xx} so $\rho_{xx} = \rho_{xx}^{\mathrm{f}}$ with $\rho_{xx}^{\mathrm{f}} = 1/\sigma_{xx}^{\mathrm{f}}$, where σ_{xx}^{f} is calculated from Eq. (5.1) using the fermionic spectral function given in Eqs. (5.2) and (5.3). Also, in Eq. (5.3), $\Delta_{\mathrm{pg}} \equiv 0$ for $T \geqslant T^*$. The fitting in Fig. 1 gives $\Gamma_0/t = 0.102$ and $b = 1.4$.

Below T^*, both the bosonic conductivity σ_{xx}^{b} and Δ_{pg} become nonzero. We calculate [67] σ_{xx}^{b} from Eqs. (3.4), (4.1), and (4.9), which depend on $\{\kappa, M_{\mathrm{pair}}, \mu_{\mathrm{pair}}\}$ in Eq. (3.4). With μ_{pair} from Eq. (4.8) and $\{\kappa, M_{\mathrm{pair}}\}$ determined from microscopic theory [47,68], the only free and adjustable parameter is the inverse lifetime of the pairs, Γ, in Eq. (3.4). We choose
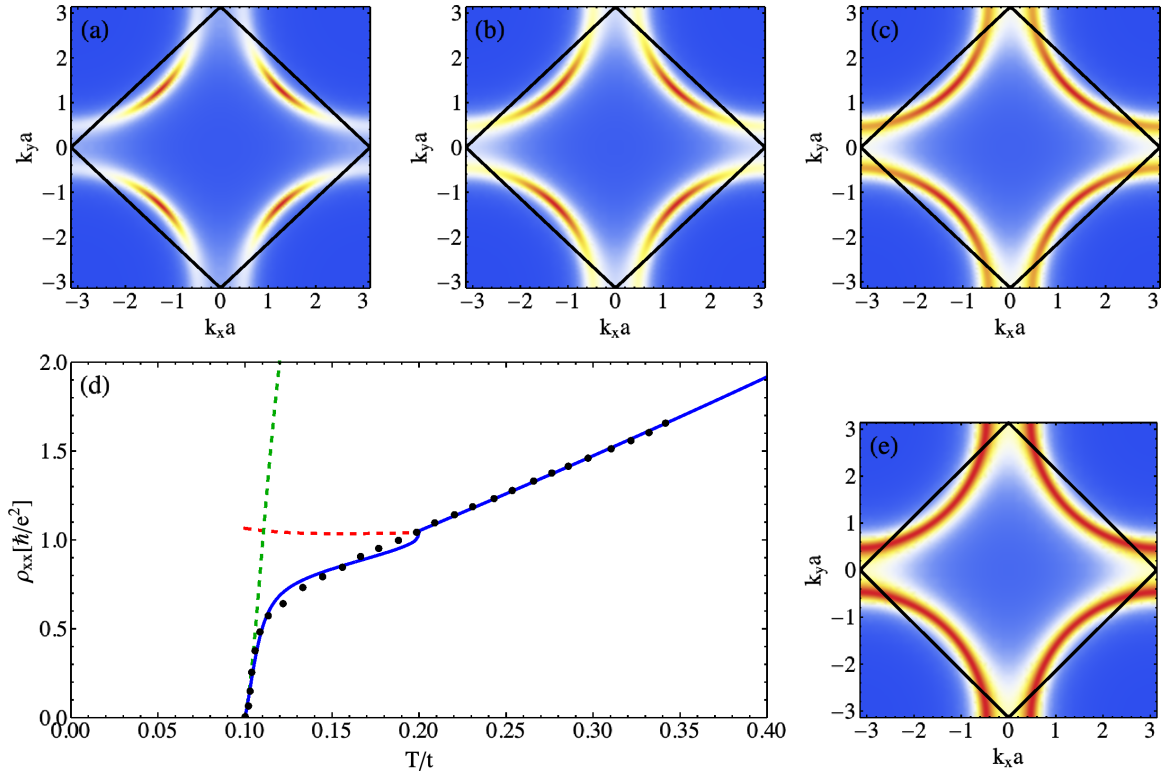
FIG. 1. Fermi arcs and fit to the resistivity of a slightly underdoped $Bi_2Sr_2CaCu_2O_{8+\delta}$ sample. Black dots in (d) are experimental data taken from Ref. [66]. The fit in (d) is shown as solid and dashed lines based on a band structure with the hopping integral $t = 75$meV. Blue solid line: Calculated total ρ_{xx}. Red dashed line: Fermionic ρ_{xx}^f. Dark green dashed line: Bosonic ρ_{xx}^b. The upturn in ρ_{xx}^f with decreasing T, relative to the linear-T background, represents the fermionic pseudogap signature which is reflected in the fermionic spectral function at the fermionic chemical potential $\mu_F(T)$, $A_f(z = 0, \mathbf{k})$. (a)–(c), (e) Representative $A_f(z = 0, \mathbf{k})$ for temperatures (a) $T/t = 0.11$, (b) $T/t = 0.15$, (c) $T/t = 0.18$, and (e) $T/t = 0.23$. Here, as in all figures, $T_c/t = 0.1$ and $T^*/t = 0.2$. The evolution shown in these figures shows that the Fermi-arc length, chosen to be reasonably consistent with photoemission, decreases with decreasing T. Note that the small kink at T^* in the theory should be viewed as an artifact; it arises from the assumed abrupt divergence in the bosonic chemical potential and the onset of the pseudogap.

the value of Γ such that the total combination of fermionic and bosonic contributions to ρ_{xx} fits the experimental ρ_{xx} at $T_c \leqslant T \leqslant T^*$ reasonably well (see Fig. 1). This leads to $\Gamma = 3$.

In Fig. 1, the fermionic contribution to the resistivity, ρ_{xx}^f (red dashed line), deviates from its linear in T background below T^* and exhibits the expected upturn as T decreases. Countering this upturn we see that the presence of bosons provides another conducting channel, which tends to increase the total $\sigma_{xx} = \sigma_{xx}^f + \sigma_{xx}^b$ and leads to a downward deviation of ρ_{xx} from its high-temperature extrapolation [69]. Very near T_c, the bosonic $\rho_{xx}^b = 1/\sigma_{xx}^b$ (green dashed line) is linear in $T - T_c$, as one can see from Eqs. (4.10a) and (4.8) [70].

C. Behavior in the conducting channels

The fundamental theoretical properties computed in this paper derive from Eqs. (3.4) and (5.1) and pertain to the conducting channel. Once we have established the resistivity fit, there is no parameter flexibility so these properties are predetermined. Using the Σ_0 and Γ determined from the ρ_{xx} fit in Fig. 1 we compute all of the other transport coefficients. The resulting behavior of σ_{xx}, σ_{xy}/B, β_{xx}, and β_{xy}/B are shown in Fig. 2.

There are some general trends in Fig. 2 that are rather universal. First, the magnitude of all fermionic conduction-like quantities (red dashed lines) at $T < T^*$ becomes smaller than their high-temperature extrapolations, due to the opening of a pseudogap. Second, the bosonic contributions to σ_{xx}, σ_{xy}/B, β_{xx} and β_{xy}/B diverge as $T \to T_c$ from above. In particular, the divergence of σ_{xx}^b leads to a noticeable feature in the ρ_{xx} plot of Fig. 1: the bosonic contribution (to conductivity) dominates that of the fermions, albeit in a limited temperature range; for a summary of the divergences of the bosonic transport contributions, see Sec. IV C.

In Fig. 3, we address other important experimentally accessible transport quantities. We have already discussed ρ_{xx}, shown in Fig. 3(a). In Figs. 3(b)-3(d), we plot the Hall coefficient R_H, the Seebeck coefficient S_{xx}, and the Nernst coefficient ν, based on the same set of parameters. We have approximated R_H, S_{xx}, and ν, using Eqs. (2.5), (2.4), and (2.6), respectively, as follows:

$$R_H \approx \frac{1}{B} \frac{\sigma_{xy}}{\sigma_{xx}^2}, \tag{6.1}$$

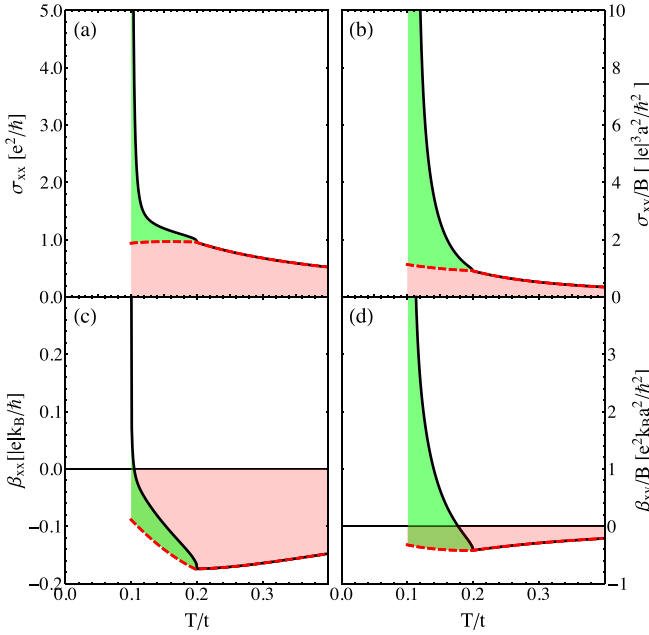$$S_{xx} \approx \frac{\beta_{xx}}{\sigma_{xx}}, \tag{6.2}$$

FIG. 2. Consequences of resistivity fits, based on Fig. 1, as seen in other transport properties. In each plot, the red dashed line and the shaded area in red represent fermionic contributions alone; while the black solid line represents the total from both fermions and bosons. The regime shaded in green reflects contributions from fluctuating Cooper pairs. Here a is the lattice constant, appearing in the units of σ_{xy}/B and β_{xy}/B. The fermionic contribution is rather small in all properties as a consequence of the bad-metal character.

$$\nu \approx \frac{1}{B}\frac{\beta_{xy}}{\sigma_{xx}}. \qquad (6.3)$$

To neglect the σ_{xy}^2 in the denominator of R_H and ν, we have restricted our focus to the weak magnetic field limit and also to T not too close to T_c such that $|\mu_{\text{pair}}| \gtrsim \omega_c^{\text{b}} = 2eB/M_{\text{pair}}$. When this latter condition is satisfied, $|\sigma_{xy}| \ll \sigma_{xx}$.

Some general features of Fig. 3 are (i) with the exception of S_{xx} and κ_{xx} all other quantities (excluding ρ_{xx}) show divergences or near-divergences in the vicinity of T_c due to their bosonic contributions. Both R_H and ν contain canceling divergences coming from the numerators and denominators of Eqs. (6.1) and (6.3), but nevertheless they lead to strong peaks in transport. (ii) The bosonic contributions are substantial over a wide temperature range above T_c, which can be also seen from Fig. 2. This derives from the fact that the fermionic conductivities (including σ_{xx}, σ_{xy}, β_{xx}, β_{xy}, κ_{xx} and κ_{xy}) are relatively small in cuprates due to their bad-metal character which in turn derives from the large value for Σ_0 in Eq. (5.3). Importantly, if one considers the case of good metals (see Appendix B) we find the bosonic contributions are confined to the rather narrow critical regime near T_c. (iii) Related to (ii), the change of the fermionic contributions across T^* due to the onset of the pseudogap is rather weak, which will be contrasted with the good-metal case where the change is quite dramatic (see Appendix B). Finally, (iv) regarding the behavior at high temperature above T^*, the quantities plotted in Fig. 3 can be divided into two groups, $\{\rho_{xx}, \nu, \kappa_{xx}/T, \kappa_{xy}/T\}$ and $\{R_H, S_{xx}\}$. The former group depends on the inverse

fermionic lifetime, Σ_0. Consequently, their magnitudes are dependent on the fact that the cuprates are bad metals. In contrast, R_H and S_{xx} do not depend on Σ_0 [71]. This is because R_H involves the ratio of σ_{xy} and σ_{xx}^2 (S_{xx} that of β_{xx} and σ_{xx}), whose dependence on this lifetime largely cancels each other.

D. Comparison to cuprate experiments

In this section, we give a summary of comparisons between our calculated transport coefficients in Fig. 3 and experimental measurements on underdoped cuprates (see Appendix C). At the outset, we identify problematic issues concerning the Hall coefficient and the thermopower which affect all theoretical attempts to understand these cuprate data and make a direct comparison between theory and experiment difficult.

Indeed, there is a sizable literature dealing with the Hall coefficient in the underdoped regime [72–80]. Among the most serious problems is that σ_{xy} is not as singular near T_c as is predicted by Gaussian fluctuation theories, where the expected singularity is stronger than in σ_{xx} (see Sec. IV C). This is presumably associated with the observation that $R_H \propto \rho_{yx}$ starts to drop with decreasing T at T slightly above T_c [74,76] and can even change its sign as T decreases toward T_c. Moreover, R_H in the normal state above T^* has a characteristic and systematic $1/T$ dependence [72,81] of unknown origin which serves as a background on top of which paraconductivity and pseudogap effects emerge.

Similarly, the normal state thermopower in underdoped cuprates [59,82–85] (at $T \sim T^*$) is positive in the experiments for the samples with the largest pseudogap. This is opposite to the band-structure predictions with a frequency and **k**-independent Σ_0 and also opposite to the sign of the Hall coefficient as has been noted previously in Refs. [23,25].

Given the easily anticipated problems outlined above for S_{xx} and R_H, comparisons between experiments and our plots are semiquantitatively reasonable only for the case of the Nernst coefficient, ν. Indeed, measurements of ν on underdoped cuprates [86–90] have a long history. However, there are some nonuniversalities concerning the Nernst effect, where there seems to be two classes of behavior. Both La$_{2-x}$Sr$_x$CuO$_4$ and Bi$_2$Sr$_2$CaCu$_2$O$_{8+\delta}$ exhibit a negative contribution to ν for $T > T^*$, which is to be associated with the fermions and their band structure. By contrast, YBa$_2$Cu$_3$O$_{6+\delta}$ and HgBa$_2$CuO$_{4+\delta}$ exhibit a positive ν at $T > T^*$ [90], inconsistent with their band structure.

In these latter compounds, ν experiences two sign changes as T drops below T^*. It changes first from positive to negative, and then back to positive at a lower T near T_c. In Ref. [90] the first sign change at higher temperature has been taken as evidence against pairing fluctuations playing an important role at $T \approx T^*$. By contrast, the experimental data of ν at $T > T_c$ in underdoped La$_{2-x}$Sr$_x$CuO$_4$ and Bi$_2$Sr$_2$CaCu$_2$O$_{8+\delta}$ [86–88,90] is rather similar to that calculated in this paper and shown in Fig. 3(d) (see Appendix C). Before arriving at any conclusions, it will be important to better understand both experimentally and theoretically the nonuniversal aspects of the Nernst data observed in the two classes of materials mentioned above.

Finally, we note that the thermal conductivities κ_{xx} or κ_{xy} do not show any distinctive features as T decreases across
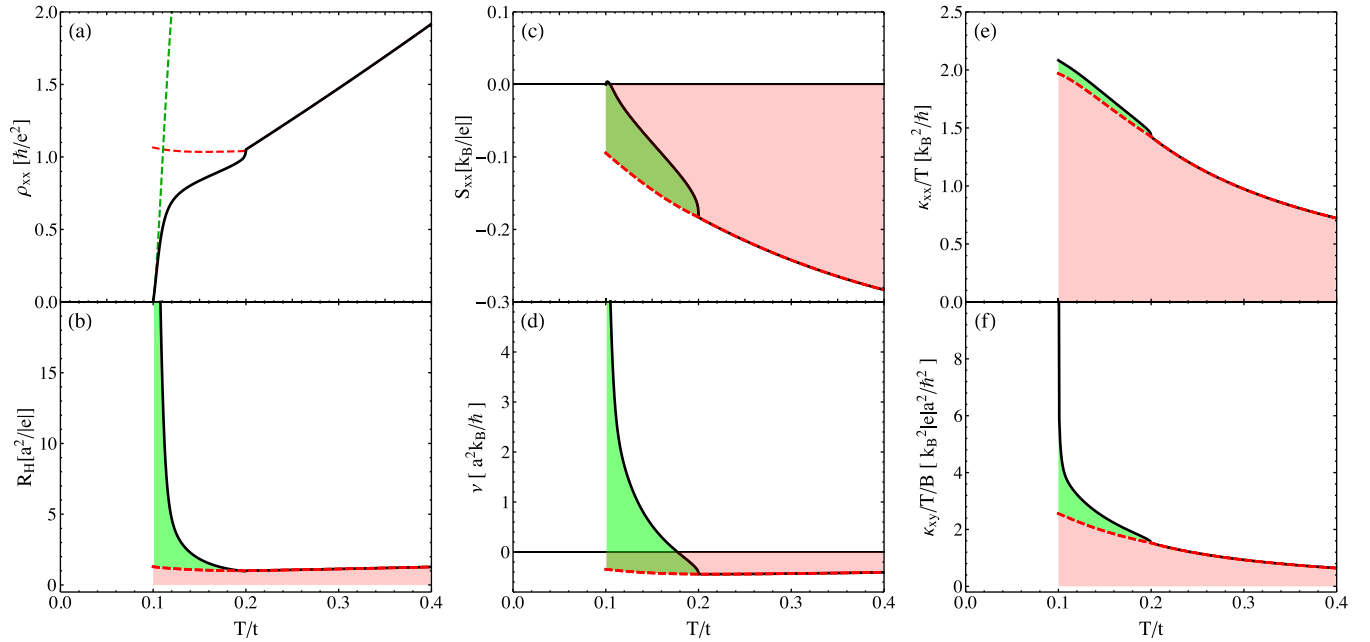
FIG. 3. Experimentally measurable transport quantities. The resistivity plot in (a) is the same as in Fig. 1, included for comparison. In all other plots, the color and line codings are the same as in Fig. 2. In this bad-metal case appropriate to the cuprates, the Cooper-pair fluctuation effects become apparent slightly below T^*.

T^*, in agreement with experiments [91,92]. Also important is the fact that the bosonic contribution to κ_{xx} and κ_{xy} at $T_c < T < T^*$ in Figs. 3(e) and 3(f) are, respectively, negligible, or only very weak. It should be noted that, experimentally, at least in κ_{xx} and possibly in κ_{xy} (for rather exotic chiral phonons), phononic contributions should play a role and can mask possible signatures from the charged particles.

We end by discussing to what extent we should view cuprate transport as universal. The onset of the pseudogap in the resistivity has been shown to be associated with both an upturn deviation from the linear background as well as a downturn signature. Here we have looked at the case of a downturn, which we interpret as suggesting that the bosonic contribution from the pseudogap dominates that coming from the fermions. We find that a fit to an alternative picture where an upturn is seen from T^* downwards [90], for example in La$_{2-x}$Sr$_x$CuO$_4$ and related cuprates, is possible only if the transition temperatures are rather low; when fitted in this way, we find that the remaining underlying transport behavior is not substantially changed. In this case, the fermions will be slightly more prominent in the vicinity of T^*.

VII. OPEN-CIRCUIT CONTRIBUTION

An anomalously large and negative value for κ_{xy} measured by Ref. [3] has led to substantial theoretical interest in the thermal Hall conductivity. The measured thermal conductivity, like the Nernst coefficient in Eq. (2.6), is determined under open-circuit conditions. As shown in Eq. (2.7), there are two terms in the expression for $\overset{\leftrightarrow}{\tilde{\kappa}}$–an intrinsic contribution arising from $\overset{\leftrightarrow}{\kappa}$ and the open-circuit contribution arising from $\overset{\leftrightarrow}{\gamma}\overset{\leftrightarrow}{\sigma}^{-1}\overset{\leftrightarrow}{\beta}$. Here we are interested in the weak magnetic field limit, and so we retain terms in the numerator of Eq. (2.8) only to linear

order in the magnetic field and in the denominator we ignore the field dependence. We also drop the term proportional to β_{xx}^2, since it is quadratic in the particle-hole symmetry breaking term of the fluctuation propagator, whereas κ_{xy} is linear in this term. With these assumptions, $\tilde{\kappa}_{xy}$ is given by

$$\tilde{\kappa}_{xy} \approx \kappa_{xy} - 2T\frac{\beta_{xx}}{\sigma_{xx}}\beta_{xy}. \tag{7.1}$$

The authors of Ref. [27] have called attention to the importance of the open-circuit correction, the second term in Eq. (7.1), which has been argued to dominate $\tilde{\kappa}_{xy}$ [93]. In this section, we present estimates, from the perspective of both our numerical calculations as well as experimental measurements, of the open-circuit correction and deduce that it is too small by about an order of magnitude to account for the observed sign change in the experimental results of Ref. [3].

Our numerical results are shown in Fig. 4. The difference associated with the open-circuit terms is reflected in the separation between the solid and dashed lines in this figure. Here the blue lines correspond to the total contributions and the red lines to those from the fermionic components. We find that the open-circuit terms are negligible except in the very narrow temperature regime when T is very close to T_c. Note that in Fig. 4 the open-circuit correction to ν is positive. This is because β_{xx} is primarily negative [as can be observed in Eq. (2.6) and Fig. 2].

We next provide numerical estimates based on experimental data from the cuprates. We define $\Delta\kappa = \overset{\leftrightarrow}{\tilde{\kappa}} - \overset{\leftrightarrow}{\kappa}$. From Eq. (7.1),

$$\frac{\Delta\kappa_{xy}}{T} \approx -2S_{xx}\beta_{xy}, \tag{7.2}$$

where we have used $S_{xx} \approx \beta_{xx}\rho_{xx}$. The value of S_{xx} and β_{xy} can be extracted from published experimental data for
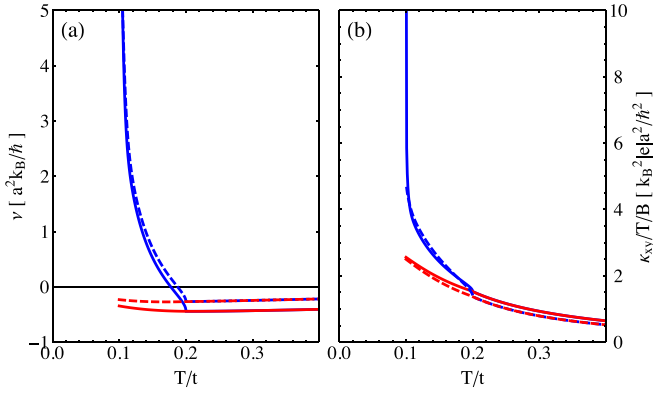
FIG. 4. Open-circuit correction terms as a comparison between $\{v, \kappa_{xy}/T/B\}$ calculated without (solid lines) and with (dashed line) these contributions for the system of Fig. 1. Red: Fermion contributions alone; blue: total contribution from both fermions and bosons. In both transport properties, the open-circuit corrections are negligibly small.

$La_{2-x}Sr_xCuO_4$ at hole doping $x \approx 0.07$, which is close to the doping level $x = 0.06$ of one sample studied in Ref. [3]. From Ref. [59], we obtain $S/T = 1.0 \, \mu V/K^2$. From Fig. 4 of Ref. [87], we infer $\beta_{xy}\rho_{xx}/B \approx 200 \, nV/(K \cdot T)$. Using $\rho_{xx} = 0.3 \, m\Omega \cdot cm$ for $x = 0.08$ from Ref. [94], we obtain $\beta_{xy}/B = 66 \, mA/(m \cdot K \cdot T)$. We use the $x = 0.08 \, \rho_{xx}$ data for our estimate since we do not expect a significant change of ρ_{xx} from $x = 0.08$ to $x = 0.07$. Inserting these values for S_{xx} and β_{xy} into Eq. (7.2) for $B = 15$ T and $T = 30$ K leads to

$$\frac{\Delta\kappa_{xy}}{T} = -0.06 \frac{mW}{m \cdot K^2}. \qquad (7.3)$$

Comparing with the corresponding experimental data [3] for $x = 0.06$ at $B = 15$ T and $T = 30$K, this appears to be too small by more than one order of magnitude to be relevant [95].

VIII. CONCLUSIONS

In this paper, we have shown how to address the broad class of fermionic and bosonic transport coefficients in a consolidated fashion in the linear magnetic field regime. Our theory is based on a reservoir approach developed for noninteracting particles. As an illustration, we applied these ideas to the normal state of the superconducting cuprates, under the hypothesis that the pseudogap phase consists simultaneously of both (gapped) fermions and bosonic pairs. This paper deals with the challenge of looking at a wide array of transport coefficients in superconductors with such a pseudogap. The challenge comes from the fact that the two types of charge carriers can have competing or enhancing contributions. Understanding which of these dominates and in which experiment is an important goal of our paper.

For the boson channel there is a general consensus that these AL-like contributions can be modeled as essentially independent bosons. Thus, the central formulas of this paper [Eq. (3.4)] are on a rather firm footing. The situation is more complicated with respect to the fermions, where the independent particle-assumption is only an approximation. In the applications to the cuprates involving fermionic contributions,

while we cannot argue that we have fully incorporated the Ward identities or gauge invariance, we do include interaction effects through the pseudogap self-energy term. This is responsible for the important Fermi arc effects. As shown in Ref. [54], the neglected vertex corrections (for the longitudinal response) are relatively small.

Most importantly, despite our more approximate treatment of the fermionic contributions, one can see from Fig. 2 that the dominant features to the transport coefficients are the bosonic contributions, which generally have a tendency to diverge or become very large. That they are so apparent over a wide range of temperatures is an important conclusion of this paper. We associate this with the bad-metal character of the cuprates which allows the bosons to be more dominant. Thus, because of this bad-metal character we do not expect a full many-body approach to qualitatively change our conclusions about transport in the cuprates.

In the process of looking at the broad class of transport coefficients, we have quantitatively studied the experimentally observed behavior of the resistivity of a prototypical under-doped cuprate. We consider the entire range of temperatures from T^* to T_c, assuming that the resistivity derives from both fermionic and fluctuating Cooper pair (bosonic) contributions. Our goal was to attribute different features in the temperature dependence to each of these two sources for charge transport and in the process provide information about the origin of the pseudogap. In the vicinity of T_c there is no question that the behavior is dominated by fluctuating Cooper pairs. Around T^*, however, there is a notably subtle feature in the resistivity data, usually a slight downturn from the linear background. We view the observation that this is so slight as very important.

Generally we can presume that the T^* signature involves both bosonic and fermionic contributions. Because the latter arise from the opening of a gap in the excitation spectrum, it is not difficult to anticipate that rather dramatic effects could be evident at T^*. Indeed, calculations in this paper suggest that it is rather challenging (see Appendices) to avoid these abrupt changes in the resistivity; it is equally problematic to arrive at *improved* conductivity (relative to the linear background) just below T^*, when this is associated with the onset of a fermionic excitation gap.

How do we understand the resistivity data, then? In our paper, we used only one adjustable parameter to fit the resistivity data and found that one can indeed recover a subtle downturn feature at T^*, but only when two key and well-known aspects of the cuprates are included: They are highly resistive or bad metals and the opening of the gap is itself rather subtle and associated with d-wave Fermi arcs. Also important is the fact that Cooper-pair fluctuations must persist, albeit weakly, up to T^*. It is important, however, to distinguish these from critical fluctuations which we find are present only very close to T_c.

What does this indicate about the origin of a pseudogap? A key finding is that this behavior in the resistivity makes it difficult to contemplate substantial changes in the fermionic spectral function associated with T^*. It is not unreasonable to assume that this quite possibly rules out new forms of order or Fermi surface reconstructions. Rather, it suggests that T^* is associated with the onset of some form of fluctuating order. Indeed, this is consistent with inferences from thermo-

dynamics where there are little or no indications of a true phase transition at T^* [33]. The presence of fluctuating order associated with the pseudogap suggests that bosonic degrees of freedom may be present and contribute to transport features at and below T^*. If the fluctuations are in the particle-particle channel and thus charged, this leads to a similar set of complications as was discussed in this paper.

In summary, there is a growing sense that understanding the full complement of thermoelectric transport properties may shed light on the still-controversial origin of the cuprate pseudogap. In contrast to the low-field limit we consider, recent emphasis has been on ultrahigh magnetic field phenomena where the superconductivity is driven away but vestiges of the pseudogap in the normal state are presumed to persist, now down to temperature $T = 0$. It remains to be seen whether this pseudogap ground state does or does not reveal the pristine normal state of the superconducting materials. Nevertheless, a clear implication is that it is important for theories to address, as we do here, the broad class of transport properties, and not just a selected few.

APPENDIX A: TRANSPORT IN CONVENTIONAL SUPERCONDUCTING FLUCTUATION THEORY

In this Appendix, we give a comparison between the conventional GL fluctuation theory in the normal-state of a superconductor [11] and the strong-pairing fluctuation theory of Sec. IV B. In addition, we provide a brief review of transport literature in the GL fluctuation theory.

1. Fluctuation propagator

We first outline how the formula given in Eq. (3.4) can be applied to the case of the GL fluctuation theory [11]. This bosonic transport encapsulates the contribution from fluctuating Cooper pairs, and in a diagrammatic framework it corresponds to the AL fluctuation diagram [11]. This approach is traditionally based on Gaussian fluctuations in the normal state, and as a result it does not directly incorporate a normal-state pseudogap.

In the GL fluctuation theory [11], the inverse fluctuation propagator is defined by

$$t_0^{-1}(p) = \sum_k G_0(k) G_0(p-k) + g^{-1}. \tag{A1}$$

Here, $p = (i\Omega_m, \mathbf{p})$ with Ω_m a bosonic Matsubara frequency. The inverse propagator can also be expressed as $t_0^{-1}(p) =$

$\Pi(p) + g^{-1}$, where $\Pi(p)$ is the pair susceptibility. The small-momentum expansion of the retarded fluctuation propagator is [11]

$$t_{0,\mathrm{R}}^{-1}(z, \mathbf{p}) = iz\gamma_{\mathrm{GL}} - \epsilon_{\mathbf{p}}. \tag{A2}$$

Here, $\gamma_{\mathrm{GL}} = \gamma_1 + i\gamma_2$ is the GL parameter and $\epsilon_{\mathbf{p}}$ is the dispersion relation for fluctuating Cooper pairs. In GL fluctuation theory, $\gamma_2 \sim T_c/E_F$ [11] where E_F is the Fermi energy, and particle-hole symmetry is only weakly broken. As a result, the transport coefficients β_{xx}, σ_{xy}, and κ_{xy}, which are proportional to γ_2, have a small prefactor.

The parameters in Eq. (A2) are given by [11]

$$\gamma_1 = \frac{\pi N_F}{8 T_c}, \tag{A3}$$

$$\gamma_2 = -\frac{1}{2} N_F \left(\frac{\partial \ln T_c}{\partial E} \right)_{E=E_F}, \tag{A4}$$

$$\epsilon_{\mathbf{p}} = N_F \left(\epsilon + \eta \mathbf{p}^2 \right). \tag{A5}$$

Here, the single-spin DOS at E_F is denoted by N_F, $\epsilon = \ln(T/T_c) \approx (T - T_c)/T_c$ and $\eta = 7\zeta(3)/(16d)[\hbar v_F/(\pi k_B T_c)]^2$ for ultraclean systems in d spatial dimensions, where v_F is the Fermi velocity. The coherence length, ξ_0, is related to η by $\xi_0^2 = \eta$; the temperature-dependent coherence length is $\xi(T) = \xi_0/\sqrt{\epsilon}$. Note that $\xi(T)$ is defined in this manner because the fluctuation regime near the critical temperature is of primary concern. In particular, the above definitions should be distinguished from the zero-temperature coherence length in BCS theory: $\xi_{\mathrm{BCS}} = \hbar v_F/(\pi \Delta_0)$ is the zero-temperature BCS coherence length and $\xi_0 \approx 0.74\xi_{\mathrm{BCS}}$ is the fluctuation coherence length, for an ultaclean three-dimensional system. In summary, all of the bosonic transport contributions in GL fluctuation theory can be determined by using Eq. (3.4), the fluctuation propagator in Eq. (A2), and the spectral function

$$A_{\mathrm{b}}(z, \mathbf{p}) = \mathrm{Re}[2it_{0,\mathrm{R}}(z, \mathbf{p})]. \tag{A6}$$

We end by summarizing the relationship between Eq. (4.1) and Eq. (A2) as follows:

$$\gamma_1 = Z\Gamma \; ; \; \gamma_2 = -Z\kappa, \tag{A7}$$

$$N_F \epsilon = Z|\mu_{\mathrm{pair}}| \; ; \; N_F \eta = Z/(2M_{\mathrm{pair}}). \tag{A8}$$

We relate the coherence lengths via $1/(2k_B T_c M_{\mathrm{pair}}) \to \eta$, and $|\mu_{\mathrm{pair}}|/(k_B T_c) \to \epsilon$. As a consequence, one can deduce the central results for the transport contributions arising from Eq. (3.4), for both GL and strong-pairing fluctuation theories, by mapping the appropriate terms.

2. Literature summary of transport results

For the benefit of the reader, here we provide a brief list of the most pertinent literature on the transport coefficients in the GL fluctuation theory. In addition to the bosonic transport of fluctuation pairs, the normal-state fluctuation theory of a superconductor contains fermionic contributions known as the MT and DOS terms [11]. The formation of fluctuating Cooper pairs causes a decrease in the density of fermions, which gives rise to the DOS term and also causes

scattering of electrons, which is respresentative of the MT term.

The AL contribution to the Nernst effect, which dominates as $T \to T_c$, was computed in Refs. [21,22] and, similarly, the contribution to the thermopower was considered by Maki [96]. The AL, MT, and DOS contributions to the longitudinal thermal conductivity were computed in Ref. [20], while the AL contribution was originally considered in Ref. [97]. The literature on the electrical conductivity is even more extensive; the MT and DOS diagrams were originally considered in Ref. [98] and, simultaneously, the AL, MT, and DOS diagrams were independently studied in Ref. [99]. For completeness, we note that the diamagnetic susceptibility was originally studied in Ref. [100] and only recently the shear viscosity has been investigated in Ref. [101]. A complete set of references can be found in Refs. [11,102].

Let us now turn to the fluctuation results for the intrinsic thermal conductivity, in the low-field limit, where there has been some initial controversy surrounding the longitudinal contribution and where the transverse contribution is more subtle. The first fluctuation calculation of longitudinal thermal conductivity was performed by Abrahams *et al.* [97]. These authors noted that the AL diagram "corresponds to the contribution of the superfluid flow to the current." Since superfluid flow produces no entropy [29] it does not transport any heat and, consequently, Abrahams *et al.* concluded that, as the critical temperature is approached, the AL diagram is expected to have zero longitudinal thermal conductivity. As a result, the main focus of these authors was the thermal response of the DOS and MT diagrams.

Later fluctuation literature [17,18,103] erroneously concluded, due to a mistreatment of the heat vertex, that the longitudinal fluctuation thermal conductivity is singular. In confirmation of the result in Ref. [97], a hydrodynamic analysis [104] argued that thermal fluctuations have a nonsingular κ_{xx}. A complete and correct microscopic calculation of κ_{xx} by Niven and Smith [20] ultimately showed that the singular contributions in the MT and DOS diagrams cancel and the AL diagram itself is nonsingular, in arbitrary dimensions and for arbitrary strengths of impurity scattering.

In subsequent work, Ussishkin *et al.* [19] correctly summarized the nature of the divergences in κ_{xy} in GL fluctuation theory and, in agreement with Ref. [20], they reported that κ_{xx} is nonsingular in two and three dimensions. We emphasize that these results and the final conclusions related to other transport coefficients are consistent with those of the present paper, as discussed in Sec. IV C. The derivation of transverse thermoelectric and transverse thermal responses requires the inclusion of magnetization currents.

While there have been numerous publications devoted to particular transport coefficients in the GL theory, there are very few papers with a unified discussion of all the transport coefficients. In Ref. [19], there is a table of the $d = 2$ and $d = 3$ results for κ and β (denoted by α in this reference). The review in Ref. [102] discusses electrical and thermoelectric conductivities, but it does not discuss thermal conductivity fluctuation results. In this paper, it is emphasized that the underlying structure of the bosonic contributions to all transport coefficients in both conventional and strong-pairing fluctuation theory can be put into the unified form con-
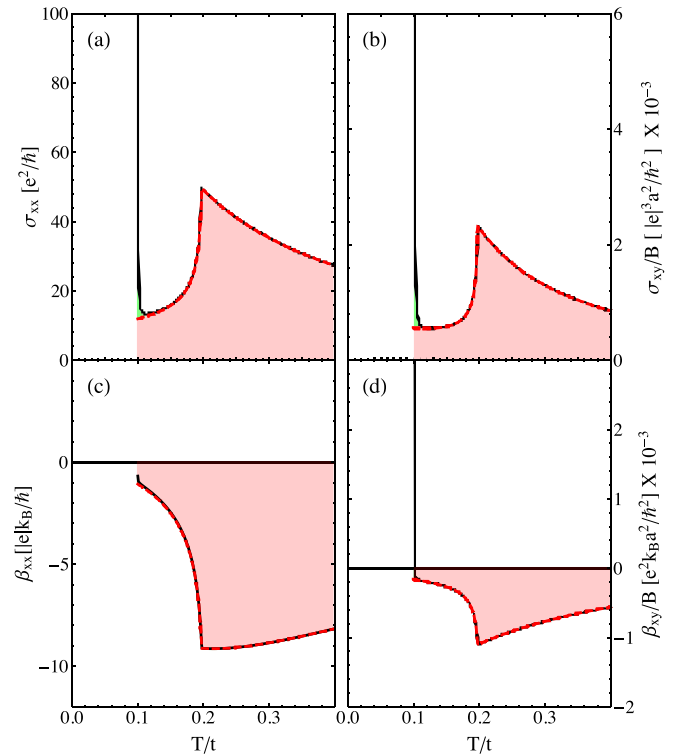

FIG. 5. Conduction properties in the good-metal case. In each plot, the red dashed line and the shaded area in red represent fermionic contributions alone, while the black solid line represents the total contribution from both fermions and bosons. The regime shaded in green stands for contributions from bosons. The fermions are quite prominent in the good-metal case.

tained in a single transport equation, Eq. (3.4), for ultraclean systems.

APPENDIX B: DETAILED COMPARISON BETWEEN BAD AND GOOD METALS

In this Appendix, we discuss the contrast between the cases of good and bad metals. This is done by varying the size of the underlying linear contribution to the resistivity, through Σ_0, for the purpose of showing what happens when the relative weight of the fermionic and bosonic contributions is changed. What is more notable in the good-metal case is that (even with Fermi arcs still present) there are now abrupt features in the fermionic contributions to transport setting in at T^*, which are in contrast to the relatively subtle features seen in experiment. Additionally, the bosonic contribution is now restricted to the more conventional critical regime, around T_c. These calculations are pedagogical, and meant to assist in understanding the more physical example of a bad metal in the main text.

Indeed, the results for the bad-metal case are already presented in Figs. 2 and 3; while those for the good metal are shown in Figs. 5 and 6. In our calculation, the good metal differs from the bad one by a 50-fold reduction of the normal-state scattering rate, Σ_0 in Eq. (5.3), while all other parameters as well as their temperature dependences remain the same [105]. This means that the absolute value of the bosonic contribution is the same for both cases.
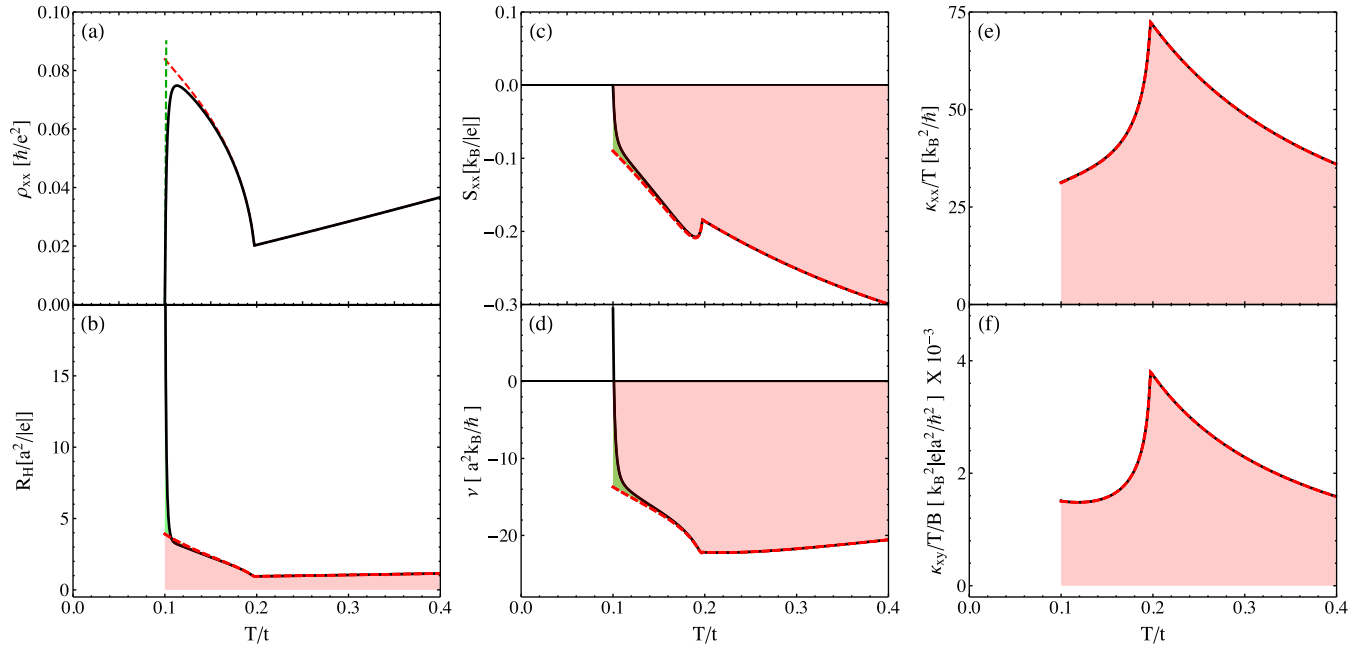
FIG. 6. Consolidated results for transport: Good-metal case. In all plots, the color and line codings are the same as in Fig. 2. The upturn in the resistivity for the good metal near T_c is driven by the fact that the fermions experience a pseudogap in their excitation spectrum and that the effective fermion scattering rate is significantly enhanced below T^* due to the Fermi arc effect (see text).

Comparing Fig. 5 to Fig. 2, we observe that one of the most important distinctions is that, in the physically more relevant bad-metal case, the bosonic contribution can be substantial even at relatively high temperatures near T^*, whereas its relevance is highly restricted to a narrow temperature range near T_c in the good-metal case. This is because from the bad to good metal, the bosonic contribution does not change while the fermionic counterpart increases by about 50 (for quantities such as σ_{xx}^f) or 50^2 (for quantities such as σ_{xy}^f/B) due to the decrease of Σ_0 in Eq. (5.3). We note that, in Fig. 5(c), β_{xx} is expected to diverge logarithmically at $T = T_c$ (see Sec. IV C), which is, however, cut off by finite-size effects in our numerical calculation.

Another distinction between Fig. 5 and Fig. 2 is that, in the good-metal case, the magnitude of all of the fermionic conductivities, $\{\sigma_{xx}^f, \sigma_{xy}^f, \beta_{xx}^f, \beta_{xy}^f\}$ (and also $\{\kappa_{xx}^f/T, \kappa_{xy}^f/T/B\}$ in Fig. 6), drops rapidly as T lowers below T^*, resulting in a cusp-like feature at T^*. This is in sharp contrast to the bad-metal case where the change in T dependence of fermionic conductivities across T^* is rather weak. The sharp drop in the good-metal case originates from an increase in the effective fermion scattering rate, which changes from Σ_0 at $T > T^*$ to $\Sigma_{0,\text{eff}} = \Sigma_0 + (\Delta_{\text{pg}}(T)\varphi_{\mathbf{k}})^2/\gamma$ [see Eq. (5.3); here, we consider $\mathbf{k} = \mathbf{k}_F$ and $\omega = 0$]. Even just slightly below T^*, $\Sigma_{0,\text{eff}} \gg \Sigma_0$ because $\Delta_{\text{pg}} \sim \gamma \gg \Sigma_0$. This rapid increase in scattering rate leads to the rapid drop of all conductivities below T^*. The effect of scattering rate change across T^* is much weaker for bad metals because there $\Sigma_0 \sim \Delta_{\text{pg}} \sim \gamma$ are all comparable.

We turn now to Fig. 6. One notable feature is that the upturn of the fermionic ρ_{xx}^f at $T < T^*$ in Fig. 6(a) is more pronounced in the good-metal case, as compared to Fig. 3(a). The sharp upturn corresponds to the rapid drop of σ_{xx}^f in Fig. 5 right below T^*.

The behaviors of R_H, S_{xx}, and ν in Fig. 6 are quite similar to those in Fig. 3 except that, for good metals, (1) the fermionic contribution to R_H has a more pronounced upturn at $T < T^*$, because $R_H^f \propto 1/n_f$ and the effect of loss of fermionic carrier density n_f is stronger, and (2) the magnitude of ν is much larger because $\nu^f \propto 1/\Sigma_0$. The similarity comes from the fact S_{xx}^f and R_H^f are rather insensitive to Σ_0.

Another similarity between Fig. 6 and Fig. 3 is that in both cases the bosonic κ_{xx}^b is negligible, which follows because κ_{xx}^b does not diverge as $T \to T_c$ in 2D (see Sec. IV C). This is in contrast to the bosonic contribution to κ_{xy}^b which shows a weak logarithmic divergence as $T \to T_c$. This divergence is not visible in Fig. 6(f) due to finite-size effects in our numerical calculations. Note also that in Fig. 6, the fermionic contributions to κ_{xx}/T and κ_{xy}/T are so large that the bosonic contributions become almost invisible.

Overall, the comparisons between Fig. 3 and Fig. 6 again underline the fact that the bosonic contributions are much more prominent over a large temperature range above T_c in the more physical case of a bad metal.

APPENDIX C: DETAILED COMPARISON BETWEEN CUPRATE DATA AND OUR THEORY

In this Appendix, we focus on qualitative temperature dependence of the transport quantities while deferring a brief discussion on their magnitudes to Appendix D.

1. Hall coefficient

We start with the Hall coefficient. There is a large body of Hall measurements on underdoped cuprates [72–80,106,107], focusing on different hole doping, temperature, and magnetic-field regimes. The Hall coefficient measured on moderately

hole-doped $YBa_2Cu_3O_{6+\delta}$ at low temperature and high magnetic field exhibits pronounced quantum oscillations [106] with a small oscillation frequency $F \sim 530$ Tesla, which corresponds to a Fermi surface area only about 2% of the Brillouin zone and suggests that the bare large holelike Fermi surface gets reconstructed.

In this paper, we focus on the weak magnetic field and high temperature ($T > T_c$) limit, where we assume no such reconstructions. In this limit, the Hall coefficient, $R_{\rm H}$, measured on underdoped cuprates shows a well-known $1/T$-dependent background [72,81], whose origin remains undetermined. One explanation [108] presumes two distinct normal-state lifetimes, one for $\sigma_{xx}^{\rm f}$ and another for $\sigma_{xy}^{\rm f}$. In our calculations, we do not consider such a distinction; instead, we use the same Σ_0 in Eq. (5.3) for both $\sigma_{xx}^{\rm f}$ and $\sigma_{xy}^{\rm f}$. Consequently, our calculated $R_{\rm H}$ in Fig. 3(b) is essentially temperature independent at $T > T^*$, as expected in a single-lifetime scenario.

The other key feature of the low-field Hall data on underdoped cuprates is that, below some characteristic T slightly above T_c, $R_{\rm H}$ decreases with decreasing T [74,76] and can even change its sign as T drops below T_c, in sharp contrast to Fig. 3(b) where $R_{\rm H}$ continues to grow as $T \to T_c$ from above. Very near T_c, our calculated $R_{\rm H}$ eventually saturates because $R_{\rm H}$ is dominated by the bosonic contribution, and it is $\propto \rho_{yx}^{\rm b} \propto \sigma_{xy}^{\rm b}/(\sigma_{xx}^{\rm b})^2$, where the divergences of $\sigma_{xy}^{\rm b}$ and $(\sigma_{xx}^{\rm b})^2$ cancel out each other (see Sec. IV C). This saturation is not shown in Fig. 3(b) because our theory is valid only for $|\mu_{\rm pair}| \propto |T - T_c| \gtrsim 2eB/M_{\rm pair}$ ($eB > 0$). Experimentally, the downturn of $R_{\rm H}$ seems to come from $\sigma_{xy}^{\rm b}$ displaying a weaker singularity than $\sigma_{xx}^{\rm b}$ as $T \to T_c$ [72,76].

An alternative way to reconcile theory with experiments is to assume that the divergent part of the bosonic $\sigma_{xy}^{\rm b}$ carries a sign opposite to that of $\sigma_{xy}^{\rm f}$ [72]. However, we emphasize that this sign, dictated by the particle-hole asymmetry factor κ in our theory (see Sec. IV C), is not arbitrary but correlated with the underlying fermionic band structure that gives rise to Cooper pairs. For the band structure we use, κ is found to be negative in Ref. [109], leading to the positive $\sigma_{xy}^{\rm b}$ in Fig. 2(b).

We could hypothesize that some additional physics due to vortices (not included in our theory), such as discussed in Ref. [110], can lead to a negative $\sigma_{xy}^{\rm b}$ and account for the downturn of $R_{\rm H}$. Future work is needed to fully resolve this issue. We note that in Ref. [111], disorder effects have been invoked to produce a divergence of $(\sigma_{xx}^{\rm b})^2$ stronger than that of $\sigma_{xy}^{\rm b}$, which leads to a downturn of ρ_{yx} near T_c in amorphous thin films. Whether this disorder mechanism is relevant in underdoped cuprates is unclear.

Although we have not been able to surmount them, we note that these challenges to transport theory are generic and not restricted to our particular physical picture.

2. Thermopower

We next consider the Seebeck (thermopower) coefficient, S_{xx}. Seebeck data on hole-doped cuprates [59,82–85] are no less puzzling than that of the Hall coefficient. For our focus on low magnetic field and $T > T_c$ in underdoped cuprates, one finds that S_{xx} shows a broad positive peak at a temperature scale $\sim T^*$ before it vanishes below T_c. In contrast, our numerical S_{xx} in Fig. 3(c) is almost entirely negative. This is a consequence of the same band structure needed to explain the Hall coefficient. A small positive contribution appears at T right above T_c and comes from the bosonic contribution which dominates at $T \approx T_c$: $S_{xx} = \beta_{xx}/\sigma_{xx} \sim \beta_{xx}^{\rm b}/\sigma_{xx}^{\rm b}$. This reflects the fact that $\beta_{xx}^{\rm b}$ is positive although the fermionic contribution $\beta_{xx}^{\rm f}$ is negative.

The issue that the observed sign of S_{xx} is opposite to what one calculates from the simple tight-binding band structure has already been noted in Refs. [23,25]. In Ref. [23], a pseudogap, whose origin is different from the one we consider here, is used to reconstruct the bare fermionic band structure in order to obtain a positive S_{xx}. However, the theory does not explain the positive S_{xx} at $T > T^*$ where the pseudogap presumably vanishes. Also considered in the literature was a frequency dependent normal state scattering rate (Σ_0 in Eq. (5.3)) or an anisotropic **k**-dependent Σ_0 [112]. In principle, both of these can lead to a sign change of S_{xx} for $T > T^*$. Recently, a frequency dependence in Σ_0 has been assumed to explain the unexpected sign of S_{xx} in a heavily overdoped cuprate [113] where one encounters a similar situation.

Although we have not been able to surmount them, we note, again, that these challenges to transport theory are generic and not restricted to our particular physical picture.

3. Nernst coefficient

Measurements of the Nernst coefficient ν on underdoped cuprates [86–90] have a long history. The experimental data of ν at $T > T_c$ in underdoped $La_{2-x}Sr_xCuO_4$ and $Bi_2Sr_2CaCu_2O_{8+\delta}$ [86–88,90] looks qualitatively similar to our results in Fig. 3(d). At $T > T^*$, ν is small and negative. Below T^* it crosses zero and exhibits a large positive peak centered at a temperature smaller than the magnetic-field dependent T_c. The peak region below T_c is usually attributed to vortex physics which is not included in our theory, while that above T_c is conventionally attributed to

TABLE I. Magnitudes of the theoretical transport quantities. While $R_{\rm H}$ at $T = T^*$ roughly agrees with the corresponding experimental data for optimally doped $Bi_2Sr_2CaCu_2O_{8+\delta}$ [77], its value at $T = 1.1T_c$ is too big. S_{xx} at $T = T^*$ has the right order of magnitude but its sign is opposite to that of underdoped $Bi_2Sr_2CaCu_2O_{8+\delta}$ [82]. Both the sign and magnitudes of ν at $T = 1.1T_c$ and $T = T^*$ are in good agreement with those of optimally doped $Bi_2Sr_2CaCu_2O_{8+\delta}$ [88]. The magnitude of κ_{xx} at the two temperatures is in rough agreement with experiments [115–117]. The theoretical κ_{xy}/B at both temperatures is an order of magnitude smaller than that observed in Ref. [92].

Quantity	$R_{\rm H}[\frac{\rm cm^3}{\rm C}]$	$S_{xx}[\frac{\mu\rm V}{\rm K}]$	$\nu[\frac{\mu\rm V}{\rm K\cdot T}]$	$\frac{\kappa_{xx}}{T}[\frac{\rm mW}{\rm K^2\cdot m}]$	$\frac{\kappa_{xy}}{TB}[\frac{\mu\rm W}{\rm K^2\cdot m\cdot T}]$
$T = 1.1T_c$	1.1×10^{-2}	-1	7×10^{-2}	4.8	2.0
$T = T^*$	7.0×10^{-4}	-16	-5×10^{-3}	3.3	0.8

TABLE II. Units used for different quantities. To obtain the second and third rows, we have used $a = 3.8$ Å, $d = 30.7/4 = 7.67$ Å for cuprates [126], where a is the in-plane lattice constant and d is the interlayer spacing per CuO$_2$ plane. Although all quantities are calculated for 2D in the main text, we switch to 3D in this table and show explicitly their dependence on the third-dimensional length scale, d, for easier comparison to experiments.

Quantity	B	σ_{xx}	σ_{xy}/B	$R_H = \frac{\rho_{yx}}{B}$	β_{xx}	β_{xy}/B	$S_{xx} = \frac{\beta_{xx}}{\sigma_{xx}}$	ν	κ_{xx}/T	$\kappa_{xy}/T/B$
Lattice unit	$\frac{\hbar}{ea^2}$	$\frac{e^2}{\hbar d}$	$\frac{e^3 a^2}{\hbar^2 d}$	$\frac{a^2 d}{|e|}$	$\frac{e k_B}{\hbar d}$	$\frac{e^2 k_B a^2}{\hbar^2 d}$	$\frac{k_B}{e}$	$\frac{a^2 k_B}{\hbar}$	$\frac{k_B^2}{\hbar d}$	$\frac{e k_B^2 a^2}{\hbar^2 d}$
Numerical value	4.56×10^3	3.17	6.96×10^{-4}	6.91×10^{-4}	27.3	6.0×10^{-3}	86.2	1.89×10^{-2}	2.36	0.52
Units	Tesla (T)	$\frac{1}{\text{m}\Omega\cdot\text{cm}}$	$\frac{1}{\text{m}\Omega\cdot\text{cm}\cdot\text{T}}$	$\frac{\text{cm}^3}{\text{C}}$	$\frac{\text{A}}{\text{K}\cdot\text{m}}$	$\frac{\text{A}}{\text{K}\cdot\text{m}\cdot\text{T}}$	$\frac{\mu\text{V}}{\text{K}}$	$\frac{\mu\text{V}}{\text{K}\cdot\text{T}}$	$\frac{\text{mW}}{\text{K}^2\cdot\text{m}}$	$\frac{\mu\text{W}}{\text{K}^2\cdot\text{m}\cdot\text{T}}$

fluctuating Cooper pairs [19,21]. Early experiments have proposed that the behavior above and below T_c may arise from fluctuating vortices [86–88], although this scenario has been challenged [114].

The Nernst data on underdoped cuprates display some non-universal characteristics. In contrast to La$_{2-x}$Sr$_x$CuO$_4$ and Bi$_2$Sr$_2$CaCu$_2$O$_{8+\delta}$, another pair of cuprates YBa$_2$Cu$_3$O$_{6+\delta}$ and HgBa$_2$CuO$_{4+\delta}$ exhibit a positive ν at $T > T^*$ [90], which is not consistent with the simple fermionic band structure. In these latter compounds, ν experiences two sign changes as T drops below T^*: it first becomes negative and then becomes positive again as T approaches T_c. In Ref. [90], the first sign change has been taken as evidence against pairing fluctuations playing an important role at $T \approx T^*$, since the contribution from fluctuating Cooper pairs is always expected to be positive. However, such a conclusion can be reached only if we better understand the origin of the variation of ν from one family to another.

In summary, our plots for ν display reasonably good agreement with experiments on La$_{2-x}$Sr$_x$CuO$_4$ and Bi$_2$Sr$_2$CaCu$_2$O$_{8+\delta}$ but are not consistent with the behavior in YBa$_2$Cu$_3$O$_{6+\delta}$ and HgBa$_2$CuO$_{4+\delta}$. This challenge to the notion of universality is an open question which (to the best of our knowledge) has not been addressed theoretically.

4. Thermal conductivities: κ_{xx} and κ_{xy}

The longitudinal thermal conductivity has a long history in the cuprate field [115–117]. The electronic contribution to κ_{xx} shows a broad peak as a function of temperature at $T < T_c$, which is believed to arise from an enhancement of the quasiparticle mean-free path as superconductivity emerges. Interestingly, κ_{xx} does not exhibit distinctive features as T decreases across T^*. This is in agreement with the theoretical plot in Fig. 3(e) which shows that the bosonic contribution is almost negligible and the fermionic contribution is very smooth.

Similarly, κ_{xy} measured at low fields [91,92,118,119] also shows a broad maximum below T_c, which is again attributed to the increase of the quasiparticle mean-free path. Much effort [120–124] has been devoted to understanding the behavior of κ_{xy} at very low T, deep in the superconducting state, where an intricate interplay between d-wave Bogoliubov quasiparticles and vortices presents a challenge to theory.

While until now there has been relatively little focus on the normal state, a series of high field κ_{xy} measurements [3,5], where the superconductivity is suppressed, were recently performed on underdoped cuprates. Here it is presumed that this will reveal the low-T and high field normal state underlying the superconducting phase as well. This high-field behavior is beyond the scope of the present paper, although establishing a baseline for the behavior even at low fields (with heat magnetization current effects included) is a useful contribution made here.

In Ref. [92], κ_{xy} was measured at low field and over a wide temperature range from $T \gtrsim T_c \sim 90$K all the way to room temperature, which is above the corresponding $T^* \sim 190$ K [125]. In this temperature regime, the observed κ_{xy}/B is well fit by a power law, $1/T^{1.2}$, with no discernible feature at T^*. The fact that the experimentally observed κ_{xy} in Ref. [92] is quite smooth at T^* seems to be consistent with our numerical results in Fig. 3(f) where the bosonic contribution to κ_{xy} is relatively small and its divergence near T_c is only logarithmic (see Sec. IV C). (This divergence can be easily cut off by other effects not included in the current treatment). Making a quantitative comparison is not possible at this stage. In particular, the small contribution from fluctuating Cooper pairs can be easily masked by chiral phonon contributions, if present. In this regard, it will be useful in the future to conduct further experiments that connect the low-field high-T regime with the high-field low-T regime.

APPENDIX D: QUANTITATIVE COMPARISON BETWEEN THEORETICAL AND EXPERIMENTAL TRANSPORT COEFFICIENTS IN THE CUPRATES

The discussions of the previous Appendix already imply that one cannot expect a general agreement between our theory and experiments over the entire temperature range. Nevertheless, in Table I, we display our theoretical values of various transport quantities in actual units for two temperatures, $T = 1.1 T_c$ and $T = T^*$. These values are obtained from Fig. 3 using the unit conversion from Table II. Table I does show that both the sign and magnitudes of the Nernst coefficient ν at $T = 1.1T_c$ and $T = T^*$ are in good agreement with those of optimally doped Bi$_2$Sr$_2$CaCu$_2$O$_{8+\delta}$[88]. In this way, a quantitative fit to the longitudinal resistivity seems to imply a good fit as well to the Nernst coefficient.

[1] Y. Kasahara, K. Sugii, T. Ohnishi, M. Shimozawa, M. Yamashita, N. Kurita, H. Tanaka, J. Nasu, Y. Motome, T. Shibauchi, and Y. Matsuda, Phys. Rev. Lett. **120**, 217205 (2018).

[2] M. Banerjee, M. Heiblum, V. Umansky, D. E. Feldman, Y. Oreg, and A. Stern, Nature (London) **559**, 205 (2018).

[3] G. Grissonnanche, A. Legros, S. Badoux, E. Lefrancóis, V. Zatko, M. Lizaire, F. Laliberté, A. Gourgout, J.-S. Zhou, S. Pyon, T. Takayama, H. Takagi, S. Ono, N. Doiron-Leyraud, and L. Taillefer, Nature (London) **571**, 376 (2019).

[4] X. Li, B. Fauqué, Z. Zhu, and K. Behnia, Phys. Rev. Lett. **124**, 105901 (2020).

[5] G. Grissonnanche, S. Thériault, A. Gourgout, M.-E. Boulanger, E. Lefrançois, A. Ataei, F. Laliberté, M. Dion, J.-S. Zhou, S. Pyon *et al.*, Nat. Phys. **16**, 1108 (2020).

[6] D. Xiao, Y. Yao, Z. Fang, and Q. Niu, Phys. Rev. Lett. **97**, 026603 (2006).

[7] Y. Kasahara, T. Ohnishi, Y. Mizukami, O. Tanaka, S. Ma, K. Sugii, N. Kurita, H. Tanaka, J. Nasu, Y. Motome, T. Shibauchi, and Y. Matsuda, Nature (London) **559**, 227 (2018).

[8] Y. N. Obraztsov, Sov. Phys. Solid State **6**, 331 (1964).

[9] N. R. Cooper, B. I. Halperin, and I. M. Ruzin, Phys. Rev. B **55**, 2344 (1997).

[10] T. Qin, Q. Niu, and J. Shi, Phys. Rev. Lett. **107**, 236601 (2011).

[11] A. I. Larkin and A. A. Varlamov, *Theory of Fluctuations in Superconductors*, International Series of Monographs on Physics (OUP, Oxford, 2009).

[12] A. O. Caldeira and A. J. Leggett, Ann. Phys. **149**, 374 (1983).

[13] J. M. Luttinger, Phys. Rev. **135**, A1505 (1964).

[14] Q. Chen, J. Stajic, S. Tan, and K. Levin, Phys. Rep. **412**, 1 (2005).

[15] S. Ullah and A. T. Dorsey, Phys. Rev. B **44**, 262 (1991).

[16] R. F. Hassing and J. W. Wilkins, Phys. Rev. B **7**, 1890 (1973).

[17] A. A. Varlamov and D. V. Livanov, Sov. Phys. JETP **71**, 325 (1990).

[18] A. A. Varlamov, L. Reggiani, and D. V. Livanov, Phys. Lett. A **165**, 369 (1992).

[19] I. Ussishkin, S. L. Sondhi, and D. A. Huse, Phys. Rev. Lett. **89**, 287001 (2002).

[20] D. R. Niven and R. A. Smith, Phys. Rev. B **66**, 214505 (2002).

[21] I. Ussishkin, Phys. Rev. B **68**, 024517 (2003).

[22] M. N. Serbyn, M. A. Skvortsov, A. A. Varlamov, and V. Galitski, Phys. Rev. Lett. **102**, 067001 (2009).

[23] J. G. Storey, J. L. Tallon, and G. V. M. Williams, Europhys. Lett. **102**, 37006 (2013).

[24] J. G. Storey, Europhys. Lett. **113**, 27003 (2016).

[25] S. Verret, O. Simard, M. Charlebois, D. Sénéchal, and A. M. S. Tremblay, Phys. Rev. B **96**, 125139 (2017).

[26] Q. Chen and K. Levin, Phys. Rev. B **78**, 020513(R) (2008).

[27] A. V. Kavokin, Y. M. Galperin, and A. A. Varlamov, Phys. Rev. Lett. **125**, 217005 (2020).

[28] J. S. Langer, Phys. Rev. **128**, 110 (1962).

[29] J. M. Luttinger, Phys. Rev. **136**, A1481 (1964).

[30] A. A. Abrikosov, *Introduction to the Theory of Normal Metals* (Academic Press, Inc., New York, 1972).

[31] J. M. Ziman, *Electrons and Phonons* (Clarendon Press, Oxford, 1960).

[32] S. Tan and K. Levin, Phys. Rev. B **69**, 064510 (2004).

[33] T. Timusk and B. Statt, Rep. Prog. Phys. **62**, 61 (1999).

[34] C. Proust and L. Taillefer, Annu. Rev. Condens. Matter Phys. **10**, 409 (2019).

[35] W. S. Lee, I. M. Vishik, K. Tanaka, D. H. Lu, T. Sasagawa, N. Nagaosa, T. P. Devereaux, Z. Hussain, and Z.-X. Shen, Nature (London) **450**, 81 (2007).

[36] Z. Dai, T. Senthil, and P. A. Lee, Phys. Rev. B **101**, 064502 (2020).

[37] M. Hashimoto, R.-H. He, K. Tanaka, J.-P. Testaud, W. Meevasana, R. G. Moore, D. Lu, Y. Yao, Y. Yoshida, H. Eisaki, T. P. Devereaux, Z. Hussain, and Z.-X. Shen, Nat. Phys. **6**, 414 (2010).

[38] A. Kanigel, U. Chatterjee, M. Randeria, M. R. Norman, G. Koren, K. Kadowaki, and J. C. Campuzano, Phys. Rev. Lett. **101**, 137002 (2008).

[39] We argue that, above T_c, one should be cautious when comparing the oversimplified BCS form of the Bogoliubov quasiparticle dispersion with that extracted from the ARPES energy distribution curves, in the absence of clear coherence peaks and given the expected large spectral broadening due to both high T and incoherent pairing processes.

[40] A. J. Leggett, in *Modern Trends in the Theory of Condensed Matter*, edited by A. Pękalski and J. A. Przystawa (Springer, Berlin, 1980), pp. 13–27.

[41] C.-C. Chien, Y. He, Q. Chen, and K. Levin, Phys. Rev. B **79**, 214527 (2009).

[42] D. Wulin, C.-C. Chien, D. K. Morr, and K. Levin, Phys. Rev. B **81**, 100504(R) (2010).

[43] V. J. Emery and S. A. Kivelson, Nature (London) **374**, 434 (1995).

[44] J. Stajic, A. Iyengar, Q. Chen, and K. Levin, Phys. Rev. B **68**, 174517 (2003).

[45] L. P. Kadanoff and P. C. Martin, Phys. Rev. **124**, 670 (1961).

[46] B. R. Patton, Phys. Rev. Lett. **27**, 1273 (1971).

[47] Q. Chen, Generalization of BCS theory to short coherence length superconductors: A BCS–Bose-Einstein crossover scenario, Ph.D. thesis, The University of Chicago, 2000.

[48] The logarithmic divergence of μ_{pair} at T^* can be motivated as follows. Assuming that Eq. (4.5) is applicable for $T > T_c$, Eq. (4.3) implies for 2D $\Delta_{\text{pg}}^2 Z = -M_{\text{pair}} T/(2\pi)\ln(1 - e^{\mu_{\text{pair}}/T})$, leading to $\mu_{\text{pair}} \propto \ln(T^* - T)$, where we have assumed that Z and M_{pair} are finite at $T \approx T^*$ and used $\Delta_{\text{pg}}^2 = \Delta_{\text{mf}}^2 \propto (T^* - T)$. Despite being well motivated, in reality the divergence of μ_{pair} at $T = T^*$ may be much less singular than logarithmic.

[49] The dimension of A_b defined in Eq. (4.9) is different from that of a usual spectral function due to the factor Z in the definition of t_R. Z carries the dimension of density of states over energy (see Eq. (A8)). However, it drops out in the calculation of the transport coefficients due to the Ward identity (see the main text).

[50] L. H. Ryder, *Quantum Field Theory*, 2nd ed. (Cambridge University Press, Cambridge, 1996).

[51] R. Boyack, Q. Chen, A. A. Varlamov, and K. Levin, Phys. Rev. B **97**, 064503 (2018).

[52] V. B. Geshkenbein, L. B. Ioffe, and A. I. Larkin, Phys. Rev. B **55**, 3173 (1997).

[53] M. R. Norman, A. Kanigel, M. Randeria, U. Chatterjee, and J. C. Campuzano, Phys. Rev. B **76**, 174501 (2007).

[54] P. Scherpelz, A. Rançon, Y. He, and K. Levin, Phys. Rev. B **90**, 060506(R) (2014).

[55] H. Kontani, Phys. Rev. B **67**, 014408 (2003).

[56] D. Wulin, B. M. Fregoso, H. Guo, C.-C. Chien, and K. Levin, Phys. Rev. B **84**, 140509(R) (2011).

[57] A. Levchenko, T. Micklitz, M. R. Norman, and I. Paul, Phys. Rev. B **82**, 060502(R) (2010).

[58] T. M. Rice, K.-Y. Yang, and F. C. Zhang, Rep. Prog. Phys. **75**, 016502 (2011).

[59] S. Badoux, S. A. A. Afshar, B. Michon, A. Ouellet, S. Fortier, D. LeBoeuf, T. P. Croft, C. Lester, S. M. Hayden, H. Takagi, K. Yamada, D. Graf, N. Doiron-Leyraud, and L. Taillefer, Phys. Rev. X **6**, 021004 (2016).

[60] S. Ono, Y. Ando, T. Murayama, F. F. Balakirev, J. B. Betts, and G. S. Boebinger, Phys. Rev. Lett. **85**, 638 (2000).

[61] Y. Ando, S. Komiya, K. Segawa, S. Ono, and Y. Kurita, Phys. Rev. Lett. **93**, 267001 (2004).

[62] N. Momono, M. Ido, T. Nakano, M. Oda, Y. Okajima, and K. Yamaya, Physica C **233**, 395 (1994).

[63] S. H. Naqib, J. R. Cooper, R. S. Islam, and J. L. Tallon, Phys. Rev. B **71**, 184510 (2005).

[64] M. R. Norman, M. Randeria, H. Ding, and J. C. Campuzano, Phys. Rev. B **57**, R11093 (1998).

[65] A. Kanigel, M. R. Norman, M. Randeria, U. Chatterjee, S. Souma, A. Kaminski, H. M. Fretwell, S. Rosenkranz, M. Shi, T. Sato, T. Takahashi, Z. Z. Li, H. Raffy, K. Kadowaki, D. Hinks, L. Ozyuzer, and J. C. Campuzano, Nat. Phys. **2**, 447 (2006).

[66] T. Watanabe, T. Fujii, and A. Matsuda, Phys. Rev. Lett. **79**, 2113 (1997).

[67] For numerical calculations, we choose the integral limit in Eq. (3.4) to be $\int_{-\pi}^{\pi} \int_{-\pi}^{\pi} \frac{d^2p}{(2\pi)^2} \int_{-5k_BT}^{5k_BT} \frac{dz}{2\pi}$.

[68] The sign of κ is related to the underlying electron band structure and filling level. In our case, $\kappa = -1$ [109].

[69] Notice that in Fig. 1, right below T^*, the total ρ_{xx} shows a sudden drop which is an artifact of our theory due to the logarithmic divergence of μ_{pair} that we used [see Eq. (4.8)].

[70] We note that had we used a different scaling for μ_{pair}, i.e., $\mu_{\text{pair}} \propto (T - T_c)^\alpha$ with α an integer >1, we would not produce the steep rise of ρ_{xx} at $T \approx T_c$, as seen experimentally. This partially justifies our choice of μ_{pair} in Eq. (4.8).

[71] For this reason, previous work by our group [109], which focused on R_H alone, did not make a distinction between the behavior of good and bad metals.

[72] J. P. Rice, J. Giapintzakis, D. M. Ginsberg, and J. M. Mochel, Phys. Rev. B **44**, 10158 (1991).

[73] H. Y. Hwang, B. Batlogg, H. Takagi, H. L. Kao, J. Kwo, R. J. Cava, J. J. Krajewski, and W. F. Peck, Phys. Rev. Lett. **72**, 2636 (1994).

[74] W. Lang, G. Heine, P. Schwab, X. Z. Wang, and D. Bäuerle, Phys. Rev. B **49**, 4209 (1994).

[75] A. V. Samoilov, Phys. Rev. B **49**, 1246 (1994).

[76] R. Jin and H. R. Ott, Phys. Rev. B **57**, 13872 (1998).

[77] Z. Konstantinović, Z. Z. Li, and H. Raffy, Phys. Rev. B **62**, R11989 (2000).

[78] D. Matthey, S. Gariglio, B. Giovannini, and J.-M. Triscone, Phys. Rev. B **64**, 024513 (2001).

[79] Y. Ando and K. Segawa, J. Phys. Chem. Solids **63**, 2253 (2002), Proceedings of the Conference on Spectroscopies in Novel Superconductors.

[80] K. Segawa and Y. Ando, Phys. Rev. B **69**, 104521 (2004).

[81] J. Clayhold, N. P. Ong, Z. Z. Wang, J. M. Tarascon, and P. Barboux, Phys. Rev. B **39**, 7324 (1989).

[82] F. Munakata, K. Matsuura, K. Kubo, T. Kawano, and H. Yamauchi, Phys. Rev. B **45**, 10604 (1992).

[83] H. Dajin, W. Ruiping, C. Weili, G. Genda, S. Qinwei, Z. Yulong, F. Juan, H. Congzhong, R. Yaozhong, and Z. Yuheng, Physica C **199**, 337 (1992).

[84] T. Fujii, I. Terasaki, T. Watanabe, and A. Matsuda, Physica C **378-381**, 182 (2002).

[85] O. Cyr-Choinière, S. Badoux, G. Grissonnanche, B. Michon, S. A. A. Afshar, S. Fortier, D. LeBoeuf, D. Graf, J. Day, D. A. Bonn, W. N. Hardy, R. Liang, N. Doiron-Leyraud, and L. Taillefer, Phys. Rev. X **7**, 031042 (2017).

[86] Z. A. Xu, N. P. Ong, Y. Wang, T. Kakeshita, and S. Uchida, Nature (London) **406**, 486 (2000).

[87] Y. Wang, Z. A. Xu, T. Kakeshita, S. Uchida, S. Ono, Y. Ando, and N. P. Ong, Phys. Rev. B **64**, 224519 (2001).

[88] Y. Wang, L. Li, and N. P. Ong, Phys. Rev. B **73**, 024510 (2006).

[89] J. Chang, N. Doiron-Leyraud, F. Laliberté, R. Daou, D. LeBoeuf, B. J. Ramshaw, R. Liang, D. A. Bonn, W. N. Hardy, C. Proust, I. Sheikin, K. Behnia, and L. Taillefer, Phys. Rev. B **84**, 014507 (2011).

[90] O. Cyr-Choinière, R. Daou, F. Laliberté, C. Collignon, S. Badoux, D. LeBoeuf, J. Chang, B. J. Ramshaw, D. A. Bonn, W. N. Hardy, R. Liang, J.-Q. Yan, J.-G. Cheng, J.-S. Zhou, J. B. Goodenough, S. Pyon, T. Takayama, H. Takagi, N. Doiron-Leyraud, and L. Taillefer, Phys. Rev. B **97**, 064502 (2018).

[91] K. Krishana, N. P. Ong, Y. Zhang, Z. A. Xu, R. Gagnon, and L. Taillefer, Phys. Rev. Lett. **82**, 5108 (1999).

[92] Y. Zhang, N. P. Ong, Z. A. Xu, K. Krishana, R. Gagnon, and L. Taillefer, Phys. Rev. Lett. **84**, 2219 (2000).

[93] In calculating the open-circuit term, the authors of Ref. [27] have identified β_{xy} with dM_z^e/dT. The latter leads to a $1/|\mu_{\text{pair}}|^2$ divergence in β_{xy}. Here M_z^e is the z component of the electric magnetization. However, as shown in Eq. (3.2), dM_z^e/dT must be combined with the microscopic current contribution, $\overleftrightarrow{L}_{e,h}$ in Eq. (3.2), to calculate β_{xy}. Our theory and that in Ref. [19] show that in the Gaussian treatment of superconducting fluctuations, the quadratic divergence is exactly cancelled between the two contributions, leading to a weaker $1/|\mu_{\text{pair}}|$ divergence in β_{xy}.

[94] S. Ono, S. Komiya, and Y. Ando, Phys. Rev. B **75**, 024515 (2007).

[95] Here we consider the case where the applied B field is small compared to B_{c2}. At larger fields, an estimate for the neglected terms shows that they are even smaller than $2S_{xx}\beta_{xy}$. We note that our open-circuit estimate in this section does not rely on the weak-field limit, although our numerical result in Sec. VI does.

[96] K. Maki, J. Low Temp. Phys. **14**, 419 (1974).

[97] E. Abrahams, M. Redi, and J. W. F. Woo, Phys. Rev. B **1**, 208 (1970).

[98] K. Maki, Prog. Theor. Phys. **40**, 193 (1968).

[99] L. G. Aslamazov and A. I. Larkin, Sov. Phys. Solid State **10**, 875 (1968).

[100] L. G. Aslamazov and A. I. Larkin, Sov. Phys. JETP **40**, 321 (1975).

[101] Y. Liao and V. Galitski, Phys. Rev. B **100**, 060501(R) (2019).

[102] A. A. Varlamov, A. Galda, and A. Glatz, Rev. Mod. Phys. **90**, 015009 (2018).

[103] A. A. Varlamov and D. V. Livanov, Sov. Phys. JETP **72**, 1016 (1991).

[104] S. Vishveshwara and M. P. A. Fisher, Phys. Rev. B **64**, 134507 (2001).

[105] We note that for good metals, ρ_{xx} typically saturates to a value smaller than the Mott-Ioffe-Regel limit at high enough temperature [127], which is violated by our good-metal model since $\Sigma_0 = \Gamma_0 + bT$ does not saturate, leading to an unsaturated ρ_{xx}. However, this is not our concern because we focus on the relatively low $T_c < T < T^*$.

[106] N. Doiron-Leyraud, C. Proust, D. LeBoeuf, J. Levallois, J.-B. Bonnemaison, R. Liang, D. A. Bonn, W. N. Hardy, and L. Taillefer, Nature (London) **447**, 565 (2007).

[107] S. Badoux, W. Tabis, F. Laliberté, G. Grissonnanche, B. Vignolle, D. Vignolles, J. Béard, D. Bonn, W. Hardy, R. Liang *et al.*, Nature (London) **531**, 210 (2016).

[108] P. W. Anderson, *The Theory of Superconductivity in the High-T_c Cuprates*, edited by S. B. Treiman (Princeton University Press, New Jersey, 1997).

[109] R. Boyack, X. Wang, Q. Chen, and K. Levin, Phys. Rev. B **99**, 134504 (2019).

[110] A. Auerbach and D. P. Arovas, SciPost Phys. **8**, 61 (2020).

[111] N. P. Breznay, K. Michaeli, K. S. Tikhonov, A. M. Finkel'stein, M. Tendulkar, and A. Kapitulnik, Phys. Rev. B **86**, 014514 (2012).

[112] N. E. Hussey, J. Phys.: Condens. Matter **20**, 123201 (2008).

[113] H. Jin, A. Narduzzo, M. Nohara, H. Takagi, N. E. Hussey, and K. Behnia, J. Phys. Soc. Jpn. **90**, 053702 (2021).

[114] K. Behnia and H. Aubin, Rep. Prog. Phys. **79**, 046502 (2016).

[115] R. C. Yu, M. B. Salamon, J. P. Lu, and W. C. Lee, Phys. Rev. Lett. **69**, 1431 (1992).

[116] P. J. Hirschfeld and W. O. Putikka, Phys. Rev. Lett. **77**, 3909 (1996).

[117] M. Sutherland, D. G. Hawthorn, R. W. Hill, F. Ronning, S. Wakimoto, H. Zhang, C. Proust, E. Boaknin, C. Lupien, L. Taillefer, R. Liang, D. A. Bonn, W. N. Hardy, R. Gagnon, N. E. Hussey, T. Kimura, M. Nohara, and H. Takagi, Phys. Rev. B **67**, 174520 (2003).

[118] B. Zeini, A. Freimuth, B. Büchner, R. Gross, A. P. Kampf, M. Kläser, and G. Müller-Vogt, Phys. Rev. Lett. **82**, 2175 (1999).

[119] Y. Zhang, N. P. Ong, P. W. Anderson, D. A. Bonn, R. Liang, and W. N. Hardy, Phys. Rev. Lett. **86**, 890 (2001).

[120] S. H. Simon and P. A. Lee, Phys. Rev. Lett. **78**, 1548 (1997).

[121] A. Vishwanath, Phys. Rev. Lett. **87**, 217004 (2001).

[122] O. Vafek, A. Melikyan, and Z. Tešanović, Phys. Rev. B **64**, 224508 (2001).

[123] A. C. Durst, A. Vishwanath, and P. A. Lee, Phys. Rev. Lett. **90**, 187002 (2003).

[124] V. Cvetkovic and O. Vafek, Nat. Commun. **6**, 6518 (2015).

[125] D. LeBoeuf, N. Doiron-Leyraud, B. Vignolle, M. Sutherland, B. J. Ramshaw, J. Levallois, R. Daou, F. Laliberté, O. Cyr-Choinière, J. Chang, Y. J. Jo, L. Balicas, R. Liang, D. A. Bonn, W. N. Hardy, C. Proust, and L. Taillefer, Phys. Rev. B **83**, 054506 (2011).

[126] V. Petricek, Y. Gao, P. Lee, and P. Coppens, Phys. Rev. B **42**, 387 (1990).

[127] O. Gunnarsson, M. Calandra, and J. E. Han, Rev. Mod. Phys. **75**, 1085 (2003).